Research

Experimental study and ANFIS modelling of the thermophysical properties and efficacy of GNP-Al$_2$O$_3$ hybrid nanofluids of different concentrations and temperatures

Adeola Borode[1] · Thato Tshephe[1] · Peter Olubambi[1] · Mohsen Sharifpur[2,3] · Josua Meyer[2,4]

Abstract

This study delves into an extensive investigation of the thermophysical properties and heat transfer efficacy of a hybrid nanofluid incorporating graphene nanoplatelets and γ-Al$_2$O$_3$ nanoparticles dispersed in deionised water. The nanofluids were characterised for their viscosity (μ), thermal conductivity (λ), and electrical conductivity (σ) over a 15–40 °C temperature range for varying nanoparticle loading (0.1–0.4 vol%). The experimental results revealed notable enhancements in μ, λ, and σ with increasing nanoparticle concentration, while μ decreased at elevated temperatures as λ and σ increased. At the highest concentration (0.4 vol%), μ increased by 21.74%, while λ and σ exhibited peak enhancements of 17.82% and 393.36% at 40 °C. An Adaptive Neuro-fuzzy Inference System (ANFIS) model was devised to enhance predictive precision by meticulously optimising the number of membership functions (MFs) and input MF type. The ANFIS architecture that exhibited the most remarkable agreement with the experimental data for μ, λ, and σ was found to utilise the Product of Sigmas, Difference of Sigmas, and Generalized Bell MFs, respectively, with corresponding input MF numbers being 2–3, 3–2, and 3–2. The optimal ANFIS model for μ, λ, and σ exhibits a higher prediction accuracy with an R^2 value of 0.99965, 0.99424 and 0.99995, respectively. The Figure of Merit analysis using Mouromtseff Number identified an optimal nanoparticle concentration range of 0.1–0.2 vol% for enhanced heat transfer performance with a reasonable μ increase. This range guides practitioners in utilising hybrid nanofluids effectively while managing potential drawbacks.

Article Highlights

- The thermophysical properties of a hybrid nanofluid incorporating GNP and γ-Al$_2$O$_3$ nanoparticles were investigated.
- The nanofluid showed significant increment in viscosity, thermal conductivity, and electrical conductivity with increasing nanoparticle concentration.
- The optimal nanoparticle concentration range for enhanced heat transfer performance with a reasonable viscosity increase was identified.

✉ Adeola Borode, hadeyola@gmail.com; aborode@uj.ac.za; ✉ Mohsen Sharifpur, mohsen.sharifpur@up.ac.za | [1]Centre for Nanoengineering and Advanced Materials, University of Johannesburg, Johannesburg, Doornfontein, South Africa. [2]Department of Mechanical and Aeronautical Engineering, University of Pretoria, Pretoria, South Africa. [3]Department of Medical Research, China Medical University Hospital, China Medical University, Taichung, Taiwan. [4]Department of Mechanical and Mechatronic Engineering, Stellenbosch University, Stellenbosch, South Africa.

Abbreviations

AAD	Average absolute deviation
AARE	Average absolute relative error
Al$_2$O$_3$	Aluminum oxide
ANFIS	Adaptive neuro-fuzzy inference system
ANN	Artificial neural network
ASHRAE	American society of heating, refrigerating, and air-conditioning engineers
COOH	Carboxyl group
CuO	Copper(II) oxide nanoparticles
DsigMF	Difference of sigmas membership function
EG	Ethylene glycol
Fe$_2$O$_3$	Iron(III) oxide nanoparticles
FIS	Fuzzy inference system
FOM	Figure of merit
GA	Genetic algorithm
GaussMF	Gaussian membership function
Gauss2MF	Double Gaussian membership function
GbellMF	Generalised Bell membership function
GO	Graphene oxide
GQDs	Graphene quantum dots
GNP	Graphene nanoplatelet
GP	Grid partitioning
LASSO	Least absolute shrinkage and selection operator
MAE	Mean absolute error
MAPE	Mean absolute percentage error
MBE	Mean bias error
MF	Membership function
MOD	Margin of deviation
MSE	Mean square error
MWCNT	Multi-walled carbon nanotubes
PiMF	Pi membership function
PsigMF	Product of sigmas membership function
RMSE	Root mean square error
SDS	Sodium dodecyl sulfate
SiC	Silicon carbide nanoparticles
SC	Subtractive clustering
SVM	Support vector machine
TH55	Therminol®55 base fluid
TiO$_2$	Titanium dioxide nanoparticles
TrapMF	Trapezoidal membership function
TriMF	Triangular membership function
a,b,c,d	Constant for mouromtseff number calculation
C	Nanoparticle concentration (vol%)
m	Mass (g)
Mo	Mouromtseff number
PPratio	Pumping power ratio
R^2	Coefficient of determination
T	Temperature (°C)
ϕ	Concentration (vol%)
λ	Thermal conductivity (W/m·K)
ρ	Density (g/cm^3)
σ	Electrical conductivity (μS/m)
μ	Viscosity (mPa·s)
ω	Weight of nanomaterial

1 Introduction

Advanced and novel coolants called nanofluids have been developed as an alternative to traditional heat transfer fluids, and they have attracted a lot of attention due to their exceptional thermal properties. Nanofluids have the potential to improve the cooling performance of heat transfer equipment due to their high heat transfer rate. These fluids are made up of nanoparticles dispersed in traditional heat transfer fluids. Numerous nanofluids with one nanoparticle have so far been created, and measurements of their thermophysical characteristics have been made [1–3]. However, recently, there has been an increase in the use of hybrid nanofluids.

Hybrid nanofluids are fluid-based suspensions of two or more different types of nanoparticles. These suspensions can be created by combining various nanofluids with various types of nanoparticles into a single hybrid nanofluid or by mixing various nanofluids with various types of nanoparticles in a single fluid. Hybrid nanofluids have been shown to stand out from other kinds of nanofluids by having special attributes that make them suitable for a range of uses, such as heat exchangers, thermal control systems, and cooling systems. When opposed to using base fluids or separate nanofluids, hybrid nanofluids provide a number of advantages. For instance, in comparison to a mono-nanofluid, the use of two or more nanoparticles can result in either a boost in thermal conductivity (λ) or a decrement in the viscosity (μ) of the nanofluids [4, 5]. This subsequently results in improved heat transfer capability. A host of studies have been conducted on different types of hybrid nanofluids [6–8].

Giwa et al. [9] studied the thermophysical properties of MWCNT-Fe$_2$O$_3$ hybrid nanofluid. They reported a maximum μ and electrical conductivity (σ) increment of approximately 36% and 1676%, respectively, compared to water. In another study by Giwa et al. [6], the thermophysical properties of Al$_2$O$_3$-MWCNT hybrid nanofluid were assessed. They observed the highest approximate increase of 26% and 19% for μ of the nanofluid with a weight ratio of 9:1 and 2:8, respectively, at the maximum temperature

of 55 °C. Gulzar et al. [10] noticed a maximum growth of 33.5% in the λ of base fluid with the addition of Al_2O_3–TiO_2 hybrid nanomaterial.

Borode et al. [11] examined the effects of concentration and temperature on the σ, μ, and λ of GNP/Fe_2O_3 hybrid nanofluids. The findings demonstrated that these nanofluids exhibit superior σ, μ, and λ compared to pure water. Notably, both σ and λ exhibited linear increments with concentration under constant temperature conditions. Meanwhile, the μ of the nanofluid increased with the incorporation of hybrid nanoparticles but decreased as temperature increased. The authors reported a maximum μ, λ and σ increment of approximately 15%, 16.83% and 351.26%.

Said et al. [12] investigated the thermophysical characteristics of hybrid nanofluids containing nanodiamond and Fe_3O_4 dispersed in water and water-ethylene glycol (EG) mixtures. Three distinct base fluids were examined: pure water, a mixture of 40% water and 60% ethylene glycol, and a mixture of 60% water and 40% EG. The hybrid nanofluids were formulated with nanodiamond + Fe_3O_4 nanoparticles at concentrations (ϕ) of 0.05%, 0.1%, and 0.2%. Results indicated significant enhancements in λ and μ for the hybrid nanofluids compared to the respective base fluids. Specifically, in pure water-based nanodiamond + Fe_3O_4 hybrid nanofluids, λ and μ improvements of 17.76% and 72.9%, respectively, were observed at a concentration (ϕ) of 0.2% and a temperature of 60 °C. Similarly, for the 40:60% water-ethylene glycol mixture-based hybrid nanofluids, the maximum enhancements of 14.65% in λ and 79.01% in μ were recorded under the same conditions. In the case of 60:40% water-ethylene glycol mixture-based hybrid nanofluids, the highest enhancements were 12.79% in λ and 50.84% in μ at $\phi = 0.2\%$ and 60 °C.

Shajan et al. [13] experimentally explore the impact of introducing graphene nanoplatelets (GNP) and alumina (Al_2O_3) nanoparticles into Therminol®55 (TH55), focusing on key thermophysical attributes such as λ, μ, and specific heat. The results highlighted significant enhancements in λ attributed to utilising hybrid nanofluids. Specifically, when compared to mono-nanofluids TH55-Al_2O_3 and TH55-GNP, the hybrid nanofluid exhibited an increase of 10.28% and 3.03%, respectively, at a temperature of 65 °C. The μ of the hybrid nanofluid exhibited an intriguing behaviour, with an initial increase of 66.99% at 20 °C compared to the base fluid, followed by a substantial decline as the temperature rose from 20 to 90 °C. The addition of nanoparticles reduced the specific heat capacity of TH55-based nanofluids due to the lower specific heat of the nanoparticles themselves.

Said et al. [14] investigated the stability and thermophysical properties of water-based hybrid nanofluids containing Fe_3O_4 material coated on MWCNT. The study employed an innovative in-situ growth approach combined with the chemical reduction method to produce Fe_3O_4-coated MWCNT. The experimentation encompassed varying particle volume loadings ranging from 0.05 to 0.3%. The findings revealed noteworthy outcomes in terms of stability and thermophysical characteristics. The highest stability with a zeta potential value of -48 mV was achieved at a particle volume loading of 0.05%. Notably, a particle volume loading of 0.3% in the hybrid nanofluid led to a substantial enhancement in λ by 13.78% and 28.33% at 20 °C and 60 °C, respectively, compared to pure water. Similarly, at the same particle volume loading of 0.3%, μ demonstrated improvements of 27.83% and 50% at 20 °C and 60 °C, respectively, compared to pure water.

Xiaoke et al. [15] investigated the heat transfer performance and distribution of thermophysical properties of ethylene glycol-based SiC-MWCNTs hybrid nanofluids as coolants in automobile engine cooling systems. By exploiting the synergistic effects of two distinct nanomaterials, the researchers achieved remarkable enhancements in λ. This enhancement was notably influenced by the concentration of nanoparticles in the fluid, showing an increasing trend with higher volume concentrations. The hybrid nanofluids exhibited a substantial maximum enhancement of 32.01% at a volume concentration of 0.4%. Notably, the flow behaviour of the SiC-MWCNTs nanofluids demonstrated Newtonian fluid characteristics. The study further examined the μ of the hybrid nanofluids and revealed a positive correlation with particle loading while showcasing a decline with rising temperatures. These favourable thermophysical properties substantially impacted the heat transfer performance of the nano-coolant.

Urmi et al. [16] present an empirical investigation into the thermophysical properties of hybrid nanofluids comprised of 40% ethylene glycol and TiO_2–Al_2O_3 nanoparticles. This study involved concentrations ranging from 0.02% to 0.1% and temperatures spanning 30–80 °C. The study's primary focus was on the μ and λ of the hybrid nanofluids compared to the base fluid. The experimental results demonstrated notable improvements in μ and λ when introducing nanoparticles. Specifically, the λ exhibited an impressive enhancement of 40.86% at a volume concentration of 0.1% and a temperature of 80 °C. Interestingly, the hybrid nanofluids exhibited higher λ than their single-component counterparts, TiO_2 and Al_2O_3, indicating a synergistic effect between the two nanoparticles. Notably, the heat transfer efficiency of the hybrid nanofluids was found to be particularly advantageous at concentrations exceeding 0.04%.

Wanatasanappan et al. [17] conducted a comprehensive study to investigate the impact of nanoparticle mixture ratios and nanofluid temperature on the λ of Al_2O_3–CuO/water-EG hybrid nanofluid. The primary objective of the research was to explore the potential for enhancing λ

through varying nanoparticle mixture ratios while considering temperature effects. A stable suspension of Al_2O_3–CuO hybrid nanofluid was prepared at different nanoparticle mixture ratios (20:80, 40:60, 50:50, and 60:40) with a fixed volume concentration of 1.0%. The λ and μ measurements were carried out across a temperature range of 30–70 °C. The study's findings indicated that the highest λ enhancement for the Al_2O_3–CuO nanofluid was achieved with a nanoparticle mixture ratio of 60:40, leading to a remarkable increase of up to 12.33% compared to the base fluid. Furthermore, the μ of the hybrid nanofluid exhibited a decreasing trend as the temperature increased.

The current landscape of nanofluid research has seen considerable exploration of various nanoparticle combinations. Yet, an intriguing and underexplored challenge remains as regards the effect of nanoparticle concentration and temperature on GNP-Al_2O_3 hybrid nanofluids. Existing literature has showcased the remarkable thermal and electrical enhancements achieved through different nanofluid compositions, such as MWCNT-Fe_2O_3 [9] and Al_2O_3-MWCNT [6] hybrid nanofluids, as well as the advantageous attributes of Al_2O_3–TiO_2 [10, 16], GNP/Fe_2O_3 [11], and nanodiamond+Fe_3O_4 [12] hybrid nanofluids. However, a noticeable research gap exists with limited attention to the thermal properties of GNP-Al_2O_3 hybrid nanofluids under the influence of concentration and temperature variations. The novelty of this work stems from its unique focus on GNP-Al_2O_3 as a hybrid nanoparticle combination, strategically selected to capitalise on GNP offering high λ and alumina, providing improved stability and dispersibility in the fluid. This strategic pairing promises enhanced heat transfer performance and points toward a compelling avenue for advancing heat management systems.

Furthermore, modelling the nanofluids' thermophysical properties is essential for applications in thermal engineering, electronics cooling, and renewable energy. However, classical models often struggle to capture the complex and non-linear behaviour of nanofluids accurately [18]. The inherent challenges arise from the intricate interplay between nanoparticle concentration, temperature, and other factors, which classical models are ill-equipped to address comprehensively. Consequently, the limitations of classical models have led researchers to turn to advanced techniques such as Adaptive Neuro-Fuzzy Inference Systems (ANFIS), Artificial Neural Networks (ANNs), Support Vector Machines (SVMs), Genetic Algorithms (GAs), among others [19], to develop more precise and efficient predictive models. These techniques mitigate the limitations of classical models in accounting for uncertainties and intricate interactions present in nanofluid systems, ultimately leading to more robust and precise property predictions for diverse thermal management applications.

For instance, Sedaghat and Yousefi [20] conducted a study focused on measuring the thermophysical properties of graphene quantum dots (GQDs) nanoparticles dispersed in various base fluids, including water, EG, and a water-EG mixture (60:40). The presence of GQDs was found to significantly enhance the μ and λ of nanofluids. Additionally, the study developed an ANN model to predict the λ and μ of these nanofluids, demonstrating excellent agreement with experimental data, achieving an AAD of 1.02% with an R^2 of 0.99929 for λ and an AAD of 1.09% with an R^2 of 0.99915 for μ.

Tian et al. [21] conducted a study utilising ANN to explore the impact of temperature and volume fraction on the λ of Graphene Oxide (GO)-Al_2O_3/water-EG hybrid nanofluid. The nanofluids were prepared with varying volume fractions of nanoparticles (ranging from 0.1% to 1.6%) and were tested across temperatures from 25 to 55 °C. The λ data was collected for six different nanoparticle volume fractions and seven different temperatures. A Perceptron feed-forward ANN was employed to create a generalised function simulating the output parameter. The results demonstrated that the ANN was effectively trained using the trainbr algorithm, yielding an average Mean Squared Error (MSE) of 1.67e−6 and a high correlation coefficient of 0.999 for λ predictions.

Yashawantha and Vinod [22] conducted experimental investigations on CuO, Al_2O_3, and TiO_2 nanofluids in an EG and water mixture to assess their λ. The nanofluid concentrations ranged from 0.2 to 2 wt%, and the study focused on low temperatures (5–25 °C). Their findings showcased a notable improvement in λ at lower temperatures. Specifically, at 5 °C, they observed enhancements of 6.34%, 4.87%, and 3.59% for CuO, Al_2O_3, and TiO_2 nanoparticles with a 2 wt% concentration compared to the EG:Water base fluid. The researchers developed correlations for effective λ based on regression analysis, considering both two-input (temperature and concentration) and three-input (temperature, concentration, and nanoparticles λ) parameters derived from experimental data. Additionally, they employed an ANFIS model to predict the effective λ of nanofluids. The ANFIS model outperformed the regression-based correlations, achieving a root mean square error (RMSE) value of 0.000712 for three input parameters compared to an RMSE of 0.00433 for the regression model. Furthermore, the ANFIS model exhibited rapid convergence during training, reaffirming its superior performance.

Zhang et al. [23] harnessed machine learning to predict crucial thermophysical properties of water-based oxide- MWCNT hybrid nanofluids, offering potential cost and time savings in experimental research. They achieved remarkable precision through rigorous optimisation of their ANFIS models using clustering techniques.

Notably, the subtractive clustering (SC)-based ANFIS model surpassed others, delivering a density prediction with an R-value of 0.99886 and a negligible Mean Absolute Percentage Error (MAPE) of 0.013%. For μ forecasting, this model again excelled, with an R-value of 0.99887 and a MAPE of 0.073%. On the other hand, the grid partitioning (GP)-based ANFIS model stood out in specific heat capacity and λ predictions, achieving an R-value of 0.99992 for specific heat capacity and an R-value of 0.99833 for λ, both with minimal MAPEs of 0.0359% and 0.0353%, respectively. This work emphasised the growing role of machine learning in nanofluid research, challenging the accuracy of conventional models and unveiling influential parameters, enhancing our understanding of nanofluids.

Vakili et al. [24] conducted a study aimed at predicting the μ of nanofluids containing graphene nanoplatelets using a multi-layered perceptron ANN coupled with a genetic algorithm (GA). Experimental data were obtained by preparing nanofluids comprising graphene nanoplatelets and deionised water at temperatures ranging from 20 to 60 °C and various weight percentages (0.025%, 0.05%, 0.075%, and 0.1% wt%). The GA was employed to optimise the ANN by selecting different weights for the connections between neurons and enhancing the bias preoccupation. To evaluate the accuracy of the proposed model's μ predictions, several performance indices, including MAPE, RMSE, R^2, and MBE, were employed. The model yielded the following values for these indices: 0.777 (MAPE), 0.086 (RMSE), 0.985 (R^2), and -0.0009 (MBE). Comparative analysis revealed that the combined model of GA and ANN aligns closely with experimental data, indicating its compatibility with empirical results. Overall, this study underscores the significance of understanding the thermophysical properties of nanofluids and investigates the hybrid performance of GA and multi-layered perceptron ANN for predicting nanofluid μ across different weight percentages and temperatures.

Sahin et al. [25] conducted a study with a primary focus on predicting the thermophysical properties of Fe_3O_4/water nanofluid, specifically targeting λ and zeta potential. Experimental measurements were conducted for nanofluid prepared at varying concentrations, and an innovative mathematical correlation was introduced to estimate λ based on temperature and concentration. Notably, this approach deviated from conventional correlations that rely solely on concentration. The research employed ANNs to predict these properties and compared their results with the experimental data. The ANN models exhibited high accuracy, with R values exceeding 0.99 and mean squared error values of 1.47E−05 and 1.58E−06 for λ and zeta potential, respectively. The average margin of deviation for λ ANN models was 0.03%, while the

new mathematical correlation achieved 0.05%. This study demonstrated the capability of ANN models to accurately predict Fe_3O_4/water nanofluid properties and highlighted their superiority over mathematical correlations in estimation accuracy. It emphasised the value of ANN models in predicting critical thermophysical properties of nanofluids without relying solely on experimental data.

Alrashed et al. [26] extensively investigated nanofluids, specifically Diamond-COOH and MWCNT-COOH nanoparticles dispersed in water without surfactants or additives. Their research spanned a temperature range of 20–50 °C and nanoparticle volume fractions (φ) from 0.0 to 0.2 vol%, focusing on thermophysical properties. In addition to traditional non-linear regression analysis, the researchers employed an ANFIS and an optimal ANN to develop predictive models. These models were trained using 70% of the 120 experimental data points, with the remaining 30% reserved for testing. Comparative evaluations were conducted, considering various theoretical models, predicted results, and experimental data. The findings revealed that the majority of theoretical models accurately define the thermophysical properties when supplied with accurate base fluid property values. MAPE and RSME were employed for model assessment. For λ, MWCNT-COOH/water nanofluids exhibited MAPE values of 0.011956 (non-linear regression), 0.00842 (ANN), and 0.16294 (ANFIS). Meanwhile, Diamond-COOH/water nanofluids displayed MAPE values of 0.04236 (non-linear regression), 0.01636 (ANN), and 0.02744 (ANFIS). In terms of density, MWCNT-COOH/water nanofluids demonstrated MAPE values of 0.00070 (non-linear regression), 0.00023 (ANN), and 0.00047 (ANFIS), while Diamond-COOH/water nanofluids exhibited MAPE values of 0.00096 (non-linear regression), 0.00054 (ANN), and 0.09998 (ANFIS). Finally, for μ, MWCNT-COOH/water nanofluids showcased MAPE values of 0.10662 (non-linear regression), 0.04617 (ANN), and 0.09275 (ANFIS), while Diamond-COOH/water nanofluids displayed MAPE values of 0.06340 (non-linear regression), 0.02877 (ANN), and 0.09894 (ANFIS). These findings highlight the effectiveness of advanced techniques, particularly ANFIS, in predicting thermophysical properties and emphasise their potential in nanofluid research and materials science.

In their study, Amani and Vajravelu [27] conducted a comprehensive assessment of ANNs for modelling the rheological and thermophysical properties of GNP-based nanofluids (CGNPs). They systematically examined different ANN structures and determined that ANNs with specific ideal neuron configurations in the hidden layer. For instance, the ANN configuration with 7 neurons for λ, 4 neurons for μ, 7 neurons for specific heat capacity, and 5 neurons for density, demonstrated optimum performance in predicting these properties with a R^2 value of 0.9996,

0.9999, 0.99998 and 0.99971, respectively. The models exhibited remarkable accuracy, with minimal MSE values and average absolute relative error (AARE) values for both training and test datasets, signifying the robustness of the ANNs in predicting nanofluid properties. The study also illustrated the close alignment between experimental and predicted results, with deviations typically within the 1–2% range. These findings underscored the suitability of ANNs for precise property prediction and highlighted the effectiveness of data partitioning and Bayesian Regularization in ensuring the ANN models' generalisation capability.

Furthermore, in the study, the prediction capabilities of LASSO and SVM methods were rigorously evaluated alongside the optimal ANN architecture using the experimental dataset. The comparative assessment of these methods reveals that all models exhibited highly comparable performance, reflecting the straightforward nature of the problem. The study noted that the differences were minimal, while the ANN models marginally outperformed SVM and LASSO in terms of MSE and R^2 values for both training and testing datasets. These findings collectively suggest that this problem lends itself to relatively simple linear models like LASSO or SVM. Consequently, the use of complex neural networks may not be imperative in practical prediction applications, such as those of cooling or heating systems involving nanofluids as the working fluid.

The extensive body of literature has emphasised the enhanced predictive attributes of all the advanced modelling techniques, including ANFIS, ANN, SVM, GA, and LASSO, among others, compared to traditional techniques. Various studies conducted by researchers [20–28] have collectively demonstrated the remarkable accuracy and effectiveness of these advanced models in predicting a wide range of thermophysical properties inherent to nanofluids. These properties encompass critical parameters such as λ, μ, density, specific heat capacity, and more. These advanced techniques have consistently outperformed traditional regression-based models and exhibited superiority over other machine-learning approaches, showcasing their prowess in terms of predictive precision and computational efficiency. However, amidst this array of advanced modelling techniques, the ANFIS stands out as particularly noteworthy. ANFIS models have consistently demonstrated their robust performance in predicting nanofluid properties, offering rapid convergence during training and remarkable precision in forecasting. This evidence, combined with the growing role of machine learning in nanofluid research and the need for highly accurate predictive models, underscores ANFIS as a compelling choice for modelling the thermophysical properties of GNP-Al$_2$O$_3$ hybrid nanofluids. It promises to provide valuable insights into the behaviour of these hybrid nanofluids under varying concentration and temperature

conditions, thereby contributing significantly to the field of thermal engineering.

Also, unlike Artificial Neural Networks (ANNs), ANFIS combines fuzzy logic and neural networks, endowing it with the ability to effectively model complex interactions between input variables (such as concentration and temperature) and output variables (λ, μ, and σ) with greater interpretability—a crucial advantage in nanofluid research, where understanding underlying physics is paramount [29, 30]. ANFIS further allows for fine-tuning of membership functions and rule structures, enhancing its adaptability to nuanced datasets. This modelling approach was deemed well-suited for the study's objectives, as it effectively accommodates the intricate and non-linear nature of nanofluid behaviour, offers interpretative insights, and demonstrates robust predictive capabilities, even with limited data.

Thus, this study aims to investigate the effect of concentration and temperature variations on the thermophysical properties and overall efficacy of GNP-Al$_2$O$_3$ hybrid nanofluids. Specifically, the nanofluid's λ, μ, and σ are measured at different nanoparticle concentrations and temperatures. Also, the heat transfer performance of the nanofluids is estimated theoretically using the Mourroseff number and the Figure-of-Merit. In addition, for the accurate prediction of the thermo-physical properties of the hybrid nanofluid, a model is developed by employing an ANFIS based on Grid Partitioning with the optimisation of hyperparameters such as number of membership functions and type of MFs.

Additionally, it is worth noting that the selection of nanoparticle concentration and temperature as the primary factors for this study was a deliberate choice to establish a strong foundational understanding of their influence on the thermophysical properties of GNP/Al$_2$O$_3$ hybrid nanofluids. These two factors were chosen for several reasons. Firstly, they represent fundamental parameters significantly impacting nanofluid behaviour and are often the starting point for nanofluid investigations. Secondly, in many practical applications, such as heat transfer systems and thermal management, the ability to control and manipulate nanoparticle concentration and temperature is more feasible and immediately relevant than controlling other factors like nanoparticle shape or the properties of the base fluid. Moreover, by focusing on these two primary variables, the authors could conduct a comprehensive and in-depth analysis within a manageable scope. Investigating all possible factors simultaneously can lead to a highly complex and resource-intensive study, and drawing meaningful conclusions from such complexity may be challenging. Thus, concentrating on concentration and temperature allowed for direct comparisons with existing literature.

This approach provides a valuable benchmark for our results and models and lays the foundation for future research that can explore the interplay of additional factors, contributing to a more holistic understanding of nanofluid behaviour.

2 Materials and methods

2.1 Experimental study

In this research, deionised water was chosen as the base fluid as it possesses higher λ and lower μ compared to other base fluids like ethylene glycol. The hybrid nanofluid was prepared using a combination of GNP and γ-Al_2O_3 nanoparticles. GNP with a thickness of 15 nm and a specific surface area of 50–80 m^2/g was procured from Sigma Aldrich (DE), while γ-Al_2O_3 with a diameter of 20–30 nm and a specific surface area of 180 m^2/g was obtained from Nanostructured & Amorphous Materials (US). SDS surfactant was employed to boost the stability of the hybrid nanofluids, with a nanoparticle-to-surfactant weight ratio of 1:1. This surfactant was also obtained from Sigma Aldrich (DE). The Eq. (1) was used to compute the weight of the nanomaterials.

$$\varphi = \frac{\omega_{GNP}\left(\frac{m}{\rho}\right)_{GNP} + \omega_{Al_2O_3}\left(\frac{m}{\rho}\right)_{Al_2O_3}}{\omega_{GNP}\left(\frac{m}{\rho}\right)_{GNP} + \omega_{Al_2O_3}\left(\frac{m}{\rho}\right)_{Al_2O_3} + \left(\frac{m}{\rho}\right)_{water}} \quad (1)$$

The hybrid nanofluids were prepared through a process involving dispersion of nanoparticles and surfactant in deionised water using a Q-700 Qsonica ultrasonic agitator for 45 min to ensure proper homogenisation. The nanofluid was placed in a temperature-controlled water bath (LAUDA ECO) during the agitation process, with a set temperature of 20 °C to avoid thermal degradation and evaporation. This method ensured that the hybrid nanofluids were well-dispersed and had a stable structure suitable for further analysis and experimentation.

The μ, λ, and σ properties of the hybrid nanofluids were assessed using the Vibro-viscometer (SV-10), KD-2 Pro meter, and EUTECH σ meter (CON700), respectively. The measurements were carried out over a temperature range of 15–40 °C, with temperature regulation provided by a water bath (LAUDA ECO). It is worth noting that the temperature range of 15–40 °C was selected to represent practical applications such as solar energy systems, electronics cooling, and HVAC systems, which often operate within this range. This choice aims to offer insights into nanofluid thermophysical properties under real-world conditions, enhancing the relevance of our findings for thermal management applications in various industries.

To ensure the accuracy and precision of our results, each measurement was repeated thrice, and the average value was taken for reporting. Statistical software was employed to fit mathematical models to the experimental data obtained from the measurements. This analytical approach enabled us to interpret and understand the data and make conclusions regarding the behaviour and properties of the hybrid nanofluids under different conditions.

Validating experimental data is crucial to assess the precision of the measurement instruments employed in this research. Measurements were conducted for the λ and μ of water to establish the experimental precision. To validate
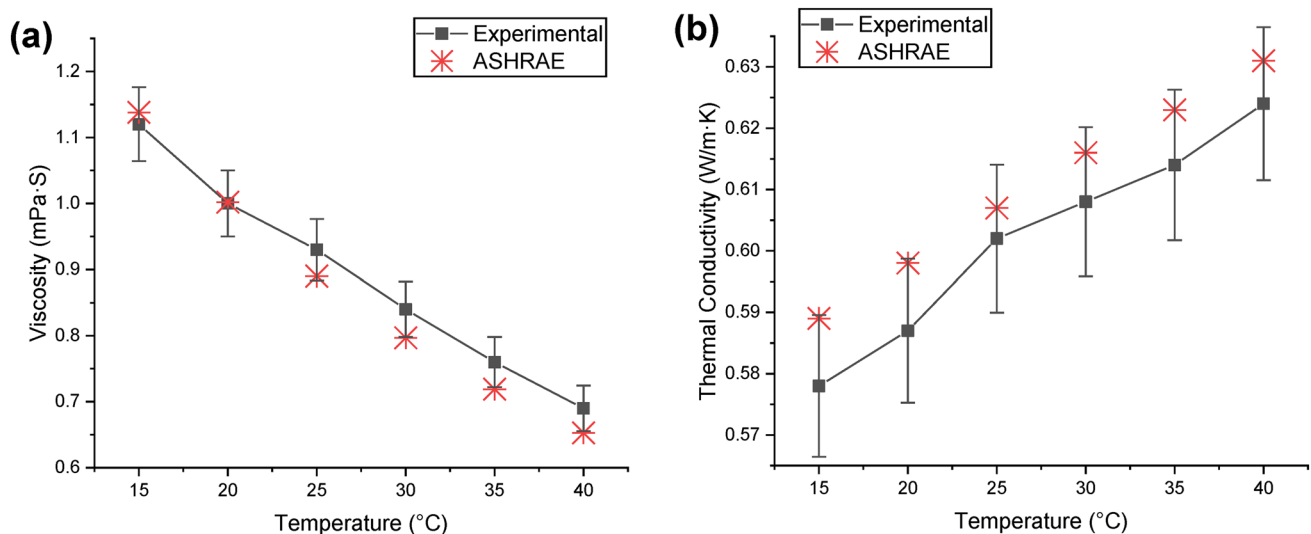

Fig. 1 Validation of the thermophysical properties of water with that of ASHRAE

the measured λ and μ, a comparison was made between the measured data and the theoretical data provided in the ASHRAE handbook [31] for water. Figure 1a presents the validation results with an error bar for μ measurements using the viscometer. The deviation in the measured data is within ± 5% when compared to ASHRAE. Also, the present λ measurement aligns well with ASHRAE with a deviation margin of about ± 1.9%. This is evident in Fig. 1b, where the validation results are presented with a 2% error bar for the λ measurements using the KD2 Pro.

The manufacturer-provided standard calibration fluid was used to calibrate the electrical conductivity meter, with three measurements taken at room temperature and an average of 1414 μS/m reported. This value was found to be similar to the manufacturer's stated value of 1413 μS/m. To ensure the accuracy of both the viscometer and KD2Pro Meter, their readings of the μ and λ were compared to the established standard values for water found in literature.

There were potential sources of error in measuring the thermophysical properties, such as inaccuracies in weighing the nanomaterials and surfactants (m), water volume, and temperature (T). These errors were taken into account by using Eq. (2) to estimate the uncertainty associated with the properties.

$$uncertainty(\%) = \pm \sqrt{\left(\frac{\partial Y}{Y}\right)^2 + \left(\frac{\partial m}{m}\right)^2 + \left(\frac{\partial V}{V}\right)^2 + \left(\frac{\partial T}{T}\right)^2}$$

(2)

The level of uncertainty associated with measuring σ is ± 2.06%, for λ it is ± 2.12%, and for μ it is ± 5.27%.

2.2 Adaptive neuro-fuzzy inference system

The ANFIS method combines fuzzy techniques with artificial neural networks to model a variety of systems. By leveraging the strengths of each approach, they complement each other and lead to a more reliable and efficient system, commonly known as neuro-fuzzy. This modelling technique was first introduced by Jang in 1993 [32]. Neuro-fuzzy logic provides a useful tool for predicting the behaviour of complex issues that are extremely difficult to model using conventional mathematical techniques. The ANFIS technique consists of five different levels [33, 34], as illustrated in Fig. 2.

In the initial layer, the input data is transformed into fuzzy inputs. These fuzzy inputs are subsequently trained using ANN methods in the second and third layers. The fuzzy IF–Then rules are then used in the fourth layer to approximate non-linear functions. Finally, in the fifth layer, the predictions are transformed from fuzzy to crisp values through defuzzification, yielding the output value.

In this study, the datasets employed for this modelling include 30 measured values each for the different
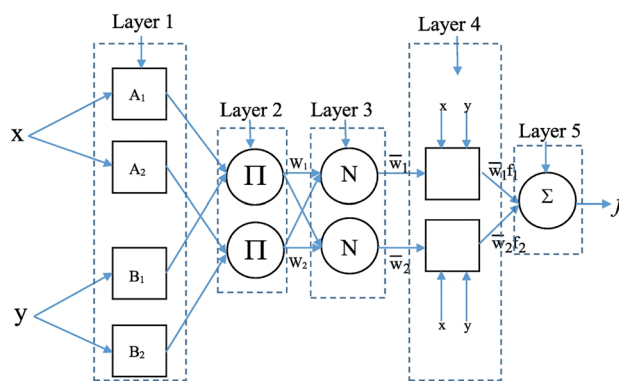

Fig. 2 Typical ANFIS architecture [35]

thermophysical properties linked to the concentration and temperature inputs. The concentration ranges from 0 to 0.4 vol% with a step increment of 0.1 vol% while the temperature ranges from 15 to 40 °C with a step increment of 5 °C. Furthermore, 80% of the data were used for training, and 20% were used for testing the ANFIS model. The data is randomly permuted to produce the training and testing datasets.

The ANFIS model in this study employs grid partitioning (GP) Sugeno-based fuzzy inference systems in MATLAB 2020a. GP-ANFIS approach is a popular technique for creating fuzzy rules, especially when working with small input variables. This technique uses membership functions (MFs) to partition the input data space into rectangular subspaces, laying the groundwork for fuzzy regions [36, 37]. An MF is assigned to each fuzzy subspace of the input. MFs can have different numbers depending on the importance and influence of the input variables.

Higher numbers of fuzzy rules in a FIS (Fuzzy Inference System) typically lead to improved performance, but it also results in higher processing costs and more complex models. Additionally, there is a limit to how many fuzzy rules may be utilised because too many rules might result in a situation where there are more changeable parameters than there are data points, which is known as the "curse of dimensionality" [38]. The number of MFs allocated to each input is limited to a specified range, which is established based on the number of accessible data points, in order to prevent running into this problem in the GP technique. This restriction makes sure that the FIS is still manageable and doesn't have the issue of having too many rules in relation to the data that is provided.

It is important to note that the number of MFs for each input, the input MF type, and the output MF type are essential structural or configuration parameters for the GP-ANFIS technique. In this study, the two inputs (concentration and temperature) are tested under 2 and 3 MF numbers each to identify the optimal combination of

input MFs. This range of MF numbers was selected because more than 3 MFs per input can increase system complexity and bring about the curse of dimensionality, while less than 2 MFs per input may result in an insufficient problem description. In order to determine the best mapping method based on input parameters, the study evaluates eight different MF types. The MF type includes Triangular (TriMF), Trapezoidal (TrapMF), Generalized Bell (GbellMF), Gaussian (GaussMF), Double Gaussian (Gauss2MF), Pi-shaped (PiMF), Difference of Sigmas (DsigMF), and Product of Sigmas (PsigMF). Also, the output MF employed in this study is linear.

Furthermore, a hybrid optimisation method is adopted for the FIS training with zero error tolerance and 100 epochs. The ANFIS modelling is performed individually for each output. Finally, the performance of the different ANFIS model configurations was evaluated using MOD, MSE, MAPE, RMSE and coefficient of determination (R^2). The equations of the various performance metrics are presented in Eqs. (3–7).

$$\text{Margin of Deviation} = \frac{\text{actual value} - \text{predicted value}}{\text{actual value}} \times 100 \tag{3}$$

Mean Absolute Percentage Error

$$= \frac{1}{n} \sum_{i=1}^{n} \left| \left(\frac{\text{actual value} - \text{predicted value}}{\text{actual value}} \times 100 \right)_i \right| \tag{4}$$

$$\text{Mean Square Error} = \frac{1}{n} \sum_{i=1}^{n} (\text{Actual Value}_i - \text{Predicted value}_i)^2 \tag{5}$$

Root Mean Square Error

$$\sqrt{\frac{1}{n} \sum_{i=1}^{n} \left(\text{Actual value}_i - \text{Predicted value}_i \right)^2} \tag{6}$$

Coefficient of Determination

$$= 1 - \frac{\sum_{i=1}^{n} (\text{Actual Value}_i - \text{Predicted value}_i)^2}{\frac{1}{n} \sum_{i=1}^{n} (\text{Actual Value}_i - \text{average value})^2} \tag{7}$$

3 Results and discussion

3.1 Optimal mixing ratio and nanofluid stability

Figure 3 displays the average λ of a 0.1 vol% hybrid GNP/Al$_2$O$_3$ nanofluid for various particle mixing ratios. The particle mixing ratio was estimated by dividing the weight of GNP by that of Al$_2$O$_3$. The findings in Fig. 3 revealed that
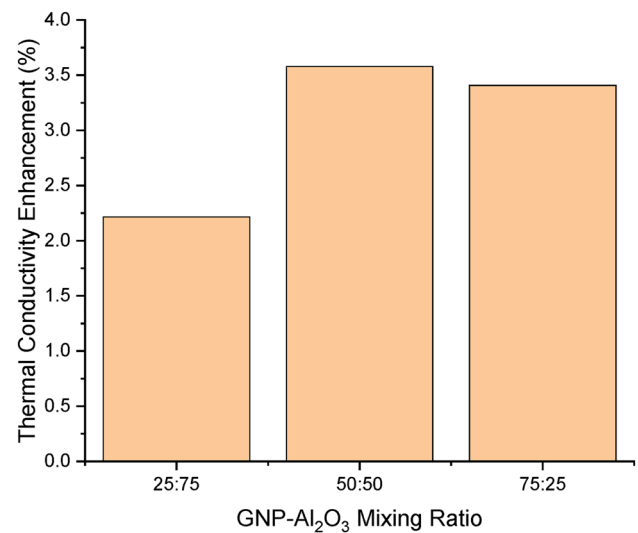

Fig. 3 Thermal conductivity enhancement of 0.1 vol% hybrid nanofluids of different GNP/Al$_2$O$_3$ mixing ratio
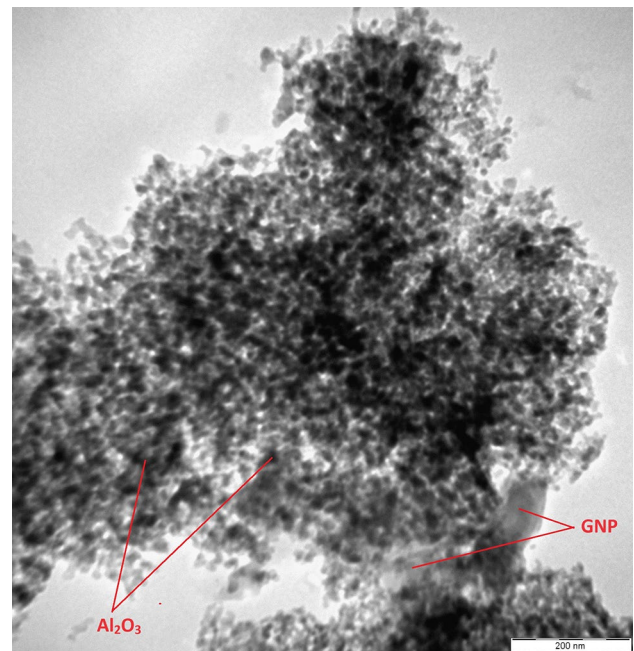

Fig. 4 TEM morphology of the hybrid nanofluid

the GNP/Al$_2$O$_3$ nanofluid with a mixture ratio of 50:50 displayed superior λ, in contrast to nanofluids with weight mixture ratios of 25:75 or (75:25). This could be as a result of the hybrid nanoparticles quickly settling in the nanofluid. As a result, a 50:50 mixing ratio by weight of GNP and Al$_2$O$_3$ nanofluid is taken into consideration for further research.
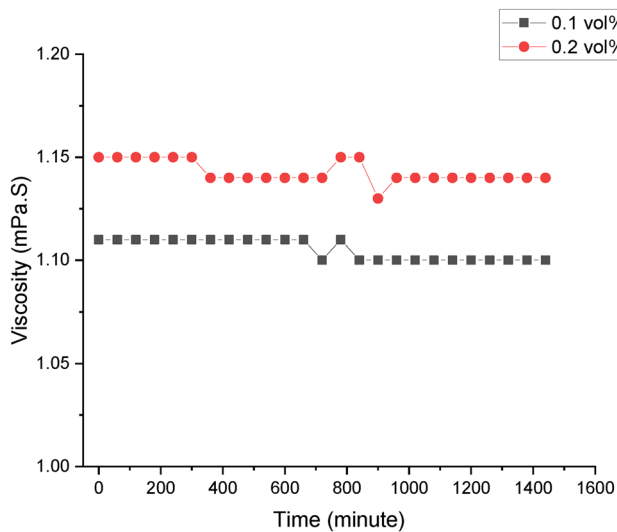
Fig. 5 Viscosity of the 0.1–0.2 vol% hybrid nanofluids over 24 h

TEM Images, μ and visual approach were utilised to assess the stability of the nanofluids. Figure 4 displays the TEM morphology of the hybrid nanofluid, which depicts the uniform dispersion of GNP and Al_2O_3 nanomaterials. Figure 5 shows the μ of the hybrid nanofluids of 0.1–0.2 vol% over 24 h. It is evident that the nanofluid exhibit good stability for up *to 24 h.*

3.2 Viscosity

Figure 6a, b illustrates the effect of temperature and GNP/Al_2O_3 concentration on the μ of the nanofluids. It can be observed that there is an increase in the μ of deionised water with the addition of the hybrid nanoparticles. Figure 6a, which illustrates the relationship between nanofluid μ and hybrid nanoparticle loading, shows that the increased addition of the nanoparticle in deionised water linearly increases the hybrid nanofluid's μ. This behaviour aligns with the established mechanisms of nanofluids, where the presence of nanoparticles can alter the fluid's rheological properties by inducing interactions and agglomeration among nanoparticles [39]. Such interactions can contribute to the formation of particle clusters that hinder the flow of the fluid, thereby resulting in higher μ. For instance, at 15 °C, the μ of the deionised water increased by 10.71% with GNP/Al_2O_3 loading of 0.1 vol%. This was further increased by 16.07% with the maximum nanoparticle loading of 0.4 vol%. This clearly indicates that the dispersion of more nanoparticles in base fluids increases the μ of nanofluids. This demonstrates unequivocally that the μ of the hybrid nanofluids increases with the dispersion of additional hybrid nanoparticles in deionised water. This increase could also be attributed to a number of variables, including a high surface-to-volume ratio of the hybrid nanoparticles and the enhanced likelihood of nanoparticles interacting rapidly.

Figure 6b, which illustrates the relationship between nanofluid μ and temperature at different hybrid nanoparticle loading, shows that an increasing temperature causes the nanofluids' μ to decline exponentially. For instance, the μ of hybrid nanofluid with nanoparticle loading of 0.1 vol% decreased by 8.06% with a temperature rise from 15 to 20 °C. A further increase to 40 °C, causes the μ to drastically reduce by 34.68%. This μ decline could be attributed to weakened intermolecular interactions between the hybrid nanoparticles and the deionised water at elevated
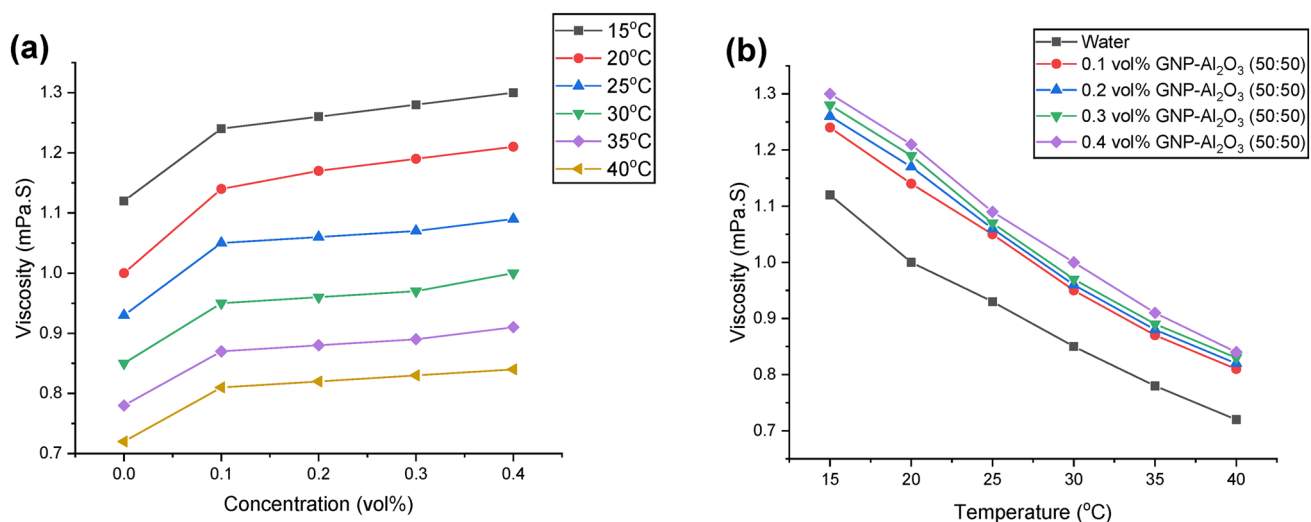

Fig. 6 Viscosity of the hybrid nanofluid in response to **a** GNP/Al_2O_3 loading and **b** temperatures

temperatures. As temperature rises, the thermal energy disrupts the structure of the fluid, reducing the resistance to flow and consequently leading to a drop in μ. This behaviour is consistent with the classical understanding of fluid dynamics and the influence of temperature on μ [40].

Finally, this study noted that the maximum μ increase of 21.74%, compared to the base fluid, is obtained with the highest nanoparticle loading of 0.4 vol% at a temperature of 40 °C. On the other hand, the lowest nanofluid μ increase of 10.71% was observed with the least particle loading of 0.1 vol% at the temperature of 15 °C. In summary, this study demonstrated that the μ of the hybrid nanofluid is directly related to GNP/Al_2O_3 loading and inversely related to temperature. This observation is similar to past research on mono-particle and hybrid nanofluids that were published in the literature [41–43]

3.3 Thermal conductivity

Figure 7a, b illustrates the impact of temperature and GNP/Al_2O_3 concentration on the λ of the nanofluids. It may be noted that there is an increase in the λ of deionised water with the addition of the hybrid nanoparticles. Figure 7a, which illustrates the relationship between nanofluid λ and hybrid nanoparticle loading, shows that the increased addition of the nanoparticle in deionised water linearly increases the hybrid nanofluid's λ. For instance, at 15 °C, the λ of the deionised water increased by 2.08% with GNP/Al_2O_3 loading of 0.1 vol%. This was further increased by 5.54% with the maximum nanoparticle loading of 0.4

vol%. This clearly indicates that the dispersion of more nanoparticles in base fluids increases the λ of nanofluids. This demonstrates unequivocally that the λ of the hybrid nanofluids increases with the dispersion of additional hybrid nanoparticles in deionised water. This phenomenon underscores the impact of a higher surface-to-volume ratio of hybrid nanoparticles and the increased probability of rapid nanoparticle interactions. The observed rise in λ can be attributed to these factors, implying the potential of the hybrid nanofluids to effectively conduct heat, which is crucial for heat transfer applications.

Figure 7b, which illustrates the relationship between nanofluid λ and temperature at different hybrid nanoparticle loading, shows that an increasing temperature causes the nanofluids' μ to decline exponentially. For instance, the λ of hybrid nanofluid with nanoparticle loading of 0.1 vol% was found to increase by 3.05% with a temperature rise from 15 to 20 °C. A further increase to 40 °C, causes the λ to increase by 10%. The observed increase in λ with elevated temperatures can be attributed to several factors, including the influence of Brownian motion [39, 44], which improves heat transfer by facilitating particle movement. This mechanism plays a significant role in the observed changes in λ at varying temperatures, underscoring the complex interplay between nanoparticle behaviour and heat transfer performance in hybrid nanofluids.

In summary, these results indicate that the maximum enhancement of 17.82% in λ is obtained with an increase in nanoparticle loading up to 0.4% at the highest temperature of 40 °C. In summary, this study demonstrated that the λ of the hybrid nanofluid is directly related to GNP/
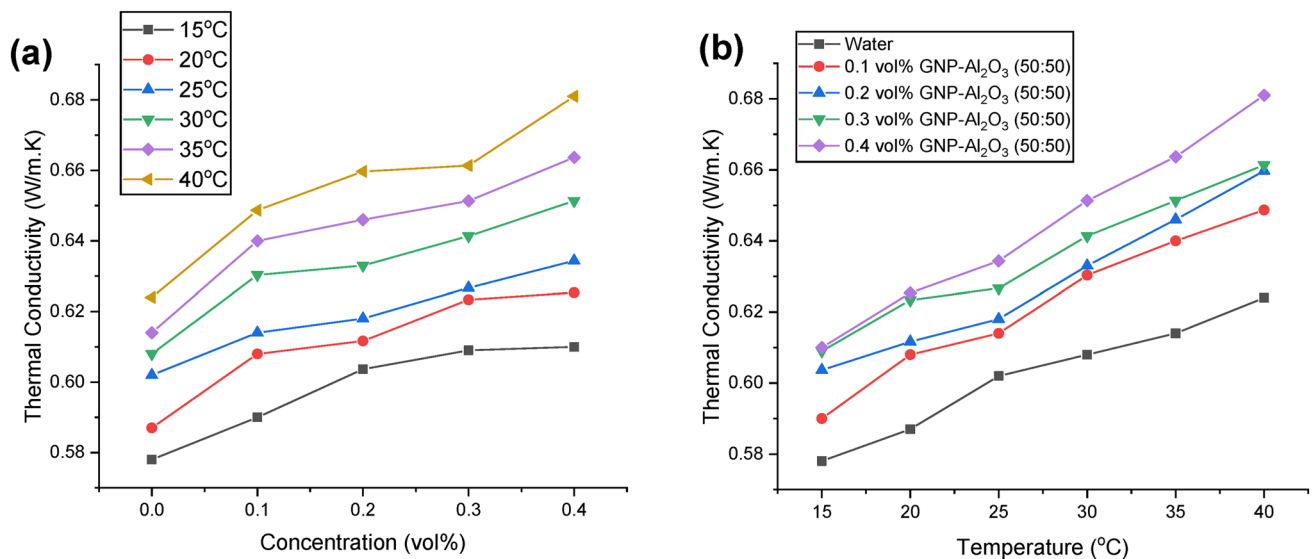

Fig. 7 Thermal Conductivity of the hybrid nanofluid in response to GNP/Al_2O_3 loading at various temperatures

Al$_2$O$_3$ loading and temperature. This observation is consistent with past research on mono-particle and hybrid nanofluids that were published in the literature [3, 45, 46]

3.4 Electrical conductivity

Electric conductivity is the ability of an aqueous solution to accommodate the transport of an electric current when a potential difference is applied. Due to the higher σ of GNP and Al$_2$O$_3$ in comparison to deionised water, the addition of these nanoparticles is expected to improve the base fluids' σ. Thus, the hybrid nanofluids of GNP- Al$_2$O$_3$ have been examined for their σ at various temperatures and concentrations, as presented in Fig. 8a, b. It was observed that the σ was linearly related to the concentration of the nanofluids. For instance, at 15 °C, the σ of the deionised water increased by 96.58% with GNP/Al$_2$O$_3$ loading of 0.1 vol%. This was further increased to the highest value by 377.99% with the maximum nanoparticle loading of 0.4 vol%. This improvement could be attributed to the enhanced amount of mobile electric charges in the nanofluid due to the presence of hybrid nanoparticles. Also, when the temperature is elevated, there was a very minor improvement in σ. The σ of hybrid nanofluid with nanoparticle loading of 0.1 vol% was found to increase by 4.15% with a temperature rise from 15 to 20 °C. A further increase to 40 °C, causes the σ to increase by 9.07%. This enhancement could be attributed to the rapid mobility of molecules at higher temperatures. This results in frequent particle collisions, which enhances the σ of the nanofluids.

Overall, this study indicates that the maximum enhancement of 393.36% in σ is obtained with an increase

in nanoparticle loading up to 0.4% at the highest temperature of 40 °C. These results established that the σ of the hybrid nanofluid is directly and linearly related to GNP/Al$_2$O$_3$ loading and temperature. This observation is in concordance with past research for mono-particle and hybrid nanofluids that were published in the literature [2, 47, 48]

3.5 Hybrid nanofluid efficacy

The Mouromtseff Number (Mo) was used to evaluate how effectively the nanofluids performed forced convective heat transfer in a thermal environment. Mo measures the thermo-effectiveness of the hybrid nanofluids in a thermal system. This depicts that increased Mo values correspond to better thermal performance. Using Eq. (8), the Mo of the samples was calculated [49].

$$Mo = \frac{\rho^a C_p^b \lambda^c}{\mu^d} \qquad (8)$$

For the turbulent flow regime of nanofluids, the constants are a = 0.8, b = 0.33, c = 0.67, and d = 0.47, while for water, they are a = 0.8, b = 0.8, c = 0.8, and d = 0.47 [50, 51].

Mo is depicted in Fig. 9a for the GNP/Al$_2$O$_3$ hybrid nanofluids for different nanoparticle loading in response to temperature. The Mo is higher at elevated temperatures for both deionised water and the hybrid nanofluids. This augmentation in Mo can be attributed to the higher λ and lower μ of the thermofluids at elevated temperatures. Also, there is a reduction in the Mo values with an increase in the nanoparticles loading from 0.1 vol% to 0.4 vol%. This is a result of the enhancement in μ.
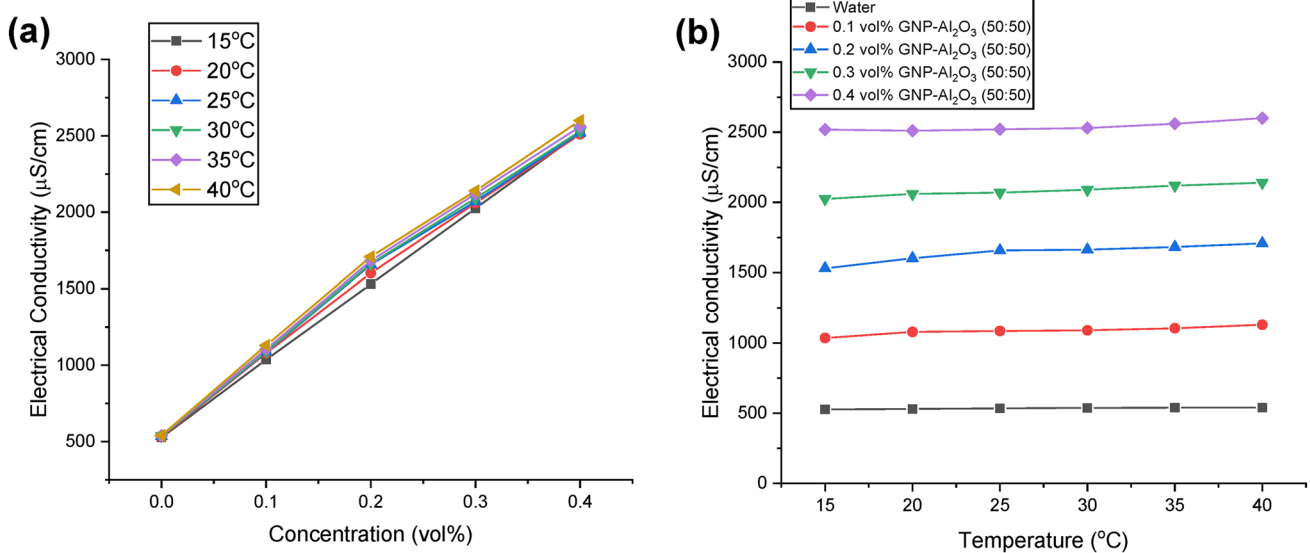

Fig. 8 Electrical Conductivity of the hybrid nanofluid in response to temperature at various GNP/Al$_2$O$_3$ concentrations
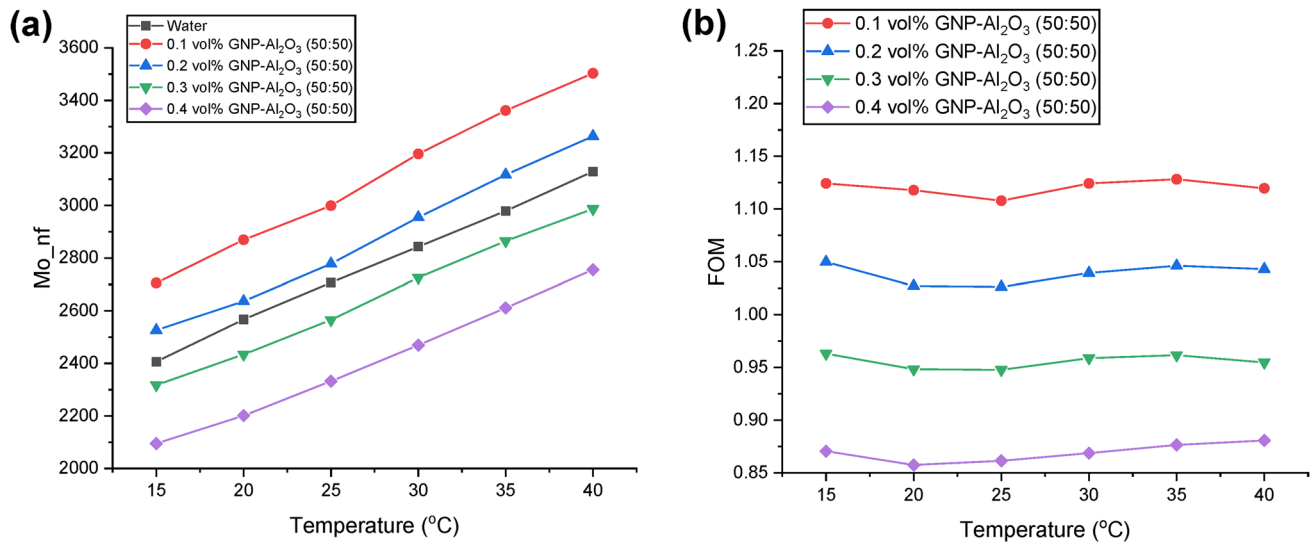
(a)

(b)

Fig. 9 **a** Mouromtseff number and **b** FOM of the GNP-Al$_2$O$_3$ hybrid nanofluids for various volume concentrations in response to temperature

Further, only hybrid nanofluids with a concentration of 0.1 vol% and 0.2 vol% have a higher Mo than the deionised water. This shows that 0.1–0.2 vol% hybrid nanofluid exhibits better thermal efficiency than water. The FOM of the hybrid nanofluids illustrated in Fig. 9b further confirms the better heat transfer efficiency of 0.1–0.2 vol% hybrid nanofluids compared to water. This is because they exhibit an FOM greater than 1, while the hybrid nanofluids with a volume concentration of exhibits a FOM lesser than 1, indicating poorer thermal efficiency compared to water.

It is crucial to remember that μ greatly impacts how well a thermal system pumps. The pumping power is anticipated to rise with increasing μ. Thus, Eq. (9) was used to calculate the pumping power ratio for the turbulent flow [50, 51].

$$PP_{ratio} = \left(\frac{\mu_{NF}}{\mu_{water}}\right)^{0.25} \left(\frac{\rho_{water}}{\rho_{NF}}\right)^2 \qquad (9)$$

The usefulness of a thermo-fluid for heat transfer is gauged by the pumping power ratio (PP$_{ratio}$). When the PP$_{ratio}$ value is lower than 1, the nanofluid is considered appropriate for heat transfer applications.

Figure 10 shows the PP$_{ratio}$ of the nanofluids at various temperatures. The PP$_{ratio}$ of the hybrid nanofluids was found to increase with an increase in concentration. However, only hybrid nanofluids with GNP/Al$_2$O$_3$ of 0.1 vol% and 0.2 vol% were discovered to be smaller than 1, proving their usefulness for heat transfer applications.

3.6 Correlation

Based on the experimental results, a novel correlation of the hybrid nanofluids was developed for the μ, λ, and σ.
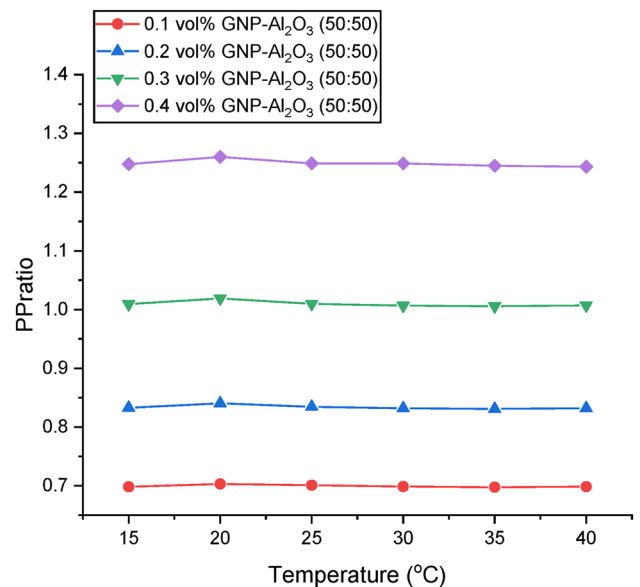

Fig. 10 PP$_{ratio}$ of the GNP-Al$_2$O$_3$ hybrid nanofluids for various volume concentrations in response to temperature

Equations (14), (15), and (16) provide the developed correlation in response to volume concentration (C) and temperature (T), respectively, with coefficients of determination (R^2) of 0.9625, 0.9585, and 0.9963.

$$Viscosity = 1.4248 - 0.017726T + 0.3450C \qquad (10)$$

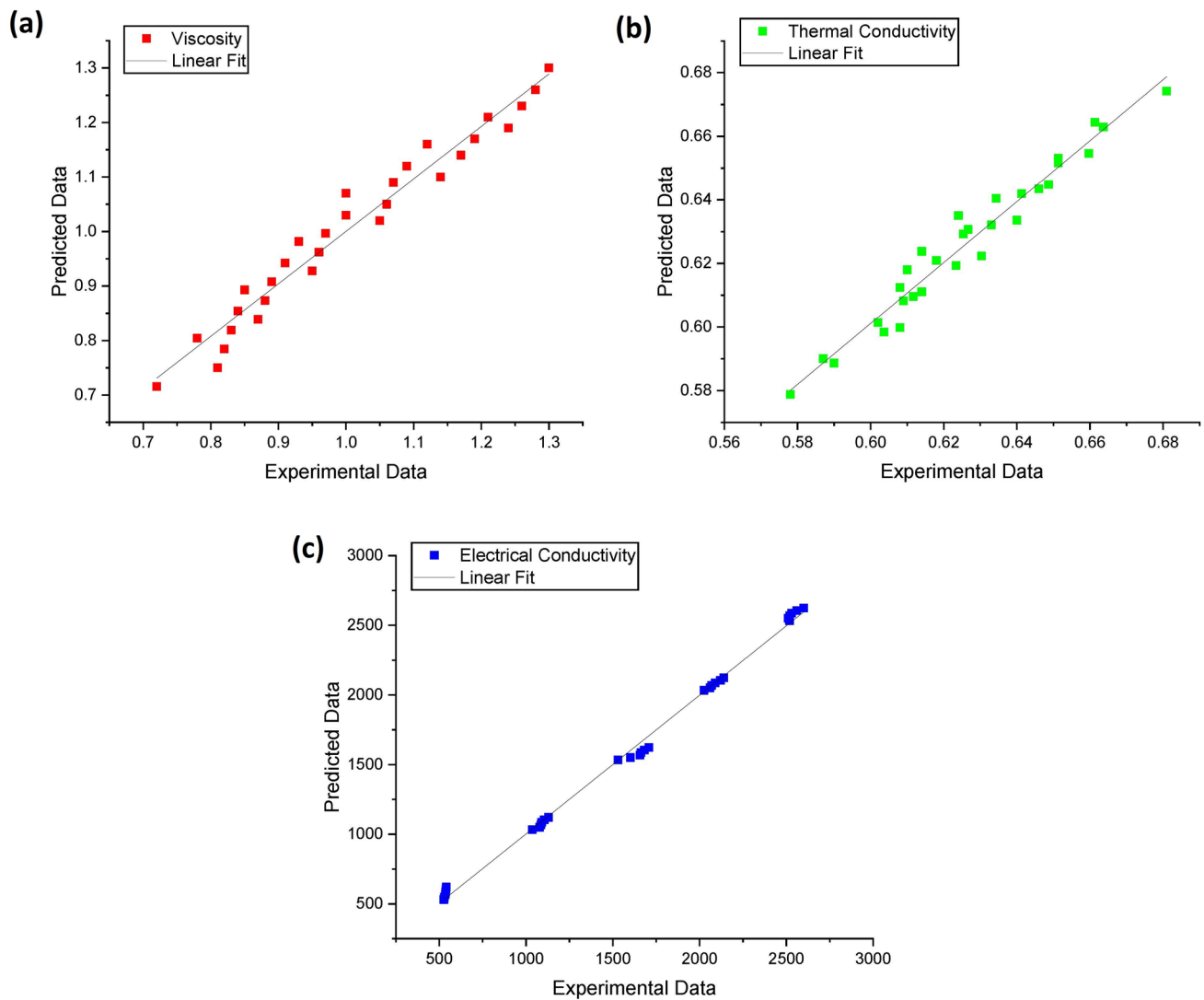$$Thermal\ Conductivity = 0.54506 + 0.002249T + 0.09788C \qquad (11)$$

Fig. 11 Linear fit of predicted and experimental data for **a** viscosity, **b** thermal conductivity, and **c** electrical conductivity

$$Electrical\ Conductivity = 477.8 + 3.568T + 5006.8C \quad (12)$$

The obtained correlation for the anticipated values of μ, λ, and σ strongly agrees with their experimental values, as shown in Fig. 11a–c. The difference between the experimental values of μ and the projected values ranges from -7.03 to 7.37%. Also, the experimental results were found to be predicted by the generated correlations for λ and σ with margins of error that ranged from -1.76 to 1.35% and -14.92 to 5.35%, respectively.

3.7 ANFIS modelling

This section examines the outcome of the effects of the number of MFs and the MF type on the performance of the two-input-one-output ANFIS architecture for the estimation of μ, λ and σ. The performance of these ANFIS architecture optimisation based on different configurations as regards the different MF types and number of MFs are presented in Tables 1, 2, and 3 for μ, λ and σ, respectively. The performance indices include the RMSE and the R^2 values, estimated for the training, testing and overall datasets as presented in the Tables. For the three

Table 1 ANFIS architecture optimisation for the nanofluid's viscosity

Run	Model	Number of MFs	RMSE			R-square		
			Training	Testing	Overall	Training	Testing	Overall
1	DsigMF	2–2	5.2082E−03	1.3871E−02	7.7578E−03	0.99896	0.99292	0.99771
2	GaussMF	2–2	4.1494E−03	9.5132E−03	5.6457E−03	0.99934	0.99667	0.99879
3	Gauss2MF	2–2	5.4594E−03	1.0170E−02	6.6730E−03	0.99886	0.99619	0.99831
4	GbellMF	2–2	4.4747E−03	1.1859E−02	6.6441E−03	0.99923	0.99482	0.99832
5	PiMF	2–2	5.4039E−03	1.1959E−02	7.2086E−03	0.99888	0.99474	0.99802
6	PsigMF	2–2	5.2082E−03	1.3871E−02	7.7578E−03	0.99896	0.99292	0.99771
7	TrapMF	2–2	5.4911E−03	8.1458E−03	6.1149E−03	0.99884	0.99756	0.99858
8	TriMF	2–2	5.9590E−03	9.6857E−03	6.8680E−03	0.99864	0.99655	0.99820
9	DsigMF	2–3	1.9381E−03	5.6432E−03	3.0617E−03	0.99986	0.99883	0.99964
10	GaussMF	2–3	1.5838E−03	1.1314E−02	5.2544E−03	0.99990	0.99529	0.99895
11	Gauss2MF	2–3	2.5923E−03	2.2589E−02	1.0365E−02	0.99974	0.98122	0.99591
12	GbellMF	2–3	1.5750E−03	1.2809E−02	5.8992E−03	0.99990	0.99396	0.99868
13	PiMF	2–3	2.5777E−03	3.9645E−02	1.7879E−02	0.99974	0.94214	0.98783
14	PsigMF	2–3	1.9383E−03	5.6238E−03	3.0547E−03	0.99986	0.99884	0.99964
15	TrapMF	2–3	2.8161E−03	2.0588E−02	9.5455E−03	0.99970	0.98440	0.99653
16	TriMF	2–3	4.2598E−03	6.3997E−03	4.7653E−03	0.99930	0.99849	0.99914
17	DsigMF	3–2	4.1042E−03	1.7660E−02	8.7092E−03	0.99935	0.98852	0.99711
18	GaussMF	3–2	3.4408E−03	1.0198E−02	5.5021E−03	0.99955	0.99617	0.99885
19	Gauss2MF	3–2	4.2462E−03	1.5162E−02	7.7719E−03	0.99931	0.99154	0.99770
20	GbellMF	3–2	3.6962E−03	1.2470E−02	6.4831E−03	0.99948	0.99428	0.99840
21	PiMF	3–2	3.9814E−03	1.7729E−02	8.6915E−03	0.99939	0.98843	0.99713
22	PsigMF	3–2	4.1042E−03	1.7660E−02	8.7091E−03	0.99935	0.98852	0.99711
23	TrapMF	3–2	4.4360E−03	1.1721E−02	6.5742E−03	0.99924	0.99494	0.99836
24	TriMF	3–2	5.0889E−03	1.0472E−02	6.5306E−03	0.99901	0.99596	0.99838

thermophysical properties, all the ANFIS configurations exhibit high reliability in the training and testing phases. Also, they exhibit very high predictive accuracies, as evidenced in the overall R^2 greater than 0.97 for all the ANFIS configurations.

Table 4 summarises the statistical performance measures of the ANFIS models. The table presents the top three best-performing ANFIS configurations for the different nanofluid properties. The selection was based on the RMSE values. ANFIS configurations with a lower RMSE are deemed to have higher performance accuracy. It can be observed that the best configuration for the prediction of the μ is with PsigMF input MF type and 2–3 number of MFs. This configuration exhibits the lowest MSE, RMSE and MAPE values with the highest R^2 value of 0.99965. On the other hand, the best configuration for λ and σ was noted to be with DsigMF and GbellMF input MF types, respectively, with similar input MF numbers of 3–2. These configurations exhibit the lowest RMSE and

MAPE values in their category and the highest R^2 values of 0.99424 and 0.99995, respectively.

To visually demonstrate the accuracy of the optimal ANFIS models, a graphical comparison between the actual and predicted values of the μ, λ, and σ of the hybrid nanofluids are presented in Figs. 12a–c and 13a–c. In Fig. 12a–c, with the predicted values plotted against the experimental values on the graph, all points align in close proximity to the straight diagonal line, signifying their high accuracy. Figure 13a–c further confirms the ability of the models to reliably estimate the nanofluids' μ, λ and σ with high accuracy.

Figure 14 presents a graph to compare the behaviour of these ANFIS models with that of the linear regression model. A closer observation of the figure reveals that the ANFIS model outperforms the linear regression model in terms of accuracy. This is because the error points for the ANFIS prediction of all the thermophysical

Table 2 ANFIS architecture optimisation for the nanofluid's thermal conductivity

Run	Model	Number of MFs	RMSE			R-square		
			Training	Testing	Overall	Training	Testing	Overall
1	DsigMF	2–2	2.3745E−03	2.1997E−03	2.3406E−03	0.99078	0.98972	0.99063
2	GaussMF	2–2	2.0755E−03	2.7840E−03	2.2352E−03	0.99296	0.98354	0.99146
3	Gauss2MF	2–2	2.1849E−03	2.5777E−03	2.2690E−03	0.99220	0.98589	0.99120
4	GbellMF	2–2	2.1176E−03	2.8973E−03	2.2948E−03	0.99267	0.98217	0.99099
5	PiMF	2–2	2.3836E−03	2.2485E−03	2.3572E−03	0.99071	0.98926	0.99050
6	PsigMF	2–2	2.3745E−03	2.1998E−03	2.3406E−03	0.99078	0.98972	0.99063
7	TrapMF	2–2	2.0457E−03	2.9200E−03	2.2479E−03	0.99316	0.98189	0.99136
8	TriMF	2–2	2.0539E−03	3.6512E−03	2.4579E−03	0.99310	0.97168	0.98967
9	DsigMF	2–3	1.7650E−03	3.9809E−03	2.3794E−03	0.99491	0.96634	0.99032
10	GaussMF	2–3	1.4646E−03	3.7993E−03	2.1454E−03	0.99649	0.96934	0.99213
11	Gauss2MF	2–3	1.4532E−03	3.6979E−03	2.1034E−03	0.99655	0.97095	0.99243
12	GbellMF	2–3	1.4245E−03	6.1691E−03	3.0389E−03	0.99668	0.91916	0.98421
13	PiMF	2–3	1.7758E−03	4.3428E−03	2.5089E−03	0.99484	0.95994	0.98923
14	PsigMF	2–3	1.7650E−03	3.9809E−03	2.3794E−03	0.99491	0.96634	0.99032
15	TrapMF	2–3	1.7694E−03	3.8463E−03	2.3374E−03	0.99488	0.96858	0.99066
16	TriMF	2–3	1.2438E−03	5.5993E−03	2.7401E−03	0.99747	0.93340	0.98716
17	DsigMF	3–2	1.5823E−03	2.6114E−03	1.8348E−03	0.99591	0.98552	0.99424
18	GaussMF	3–2	1.5904E−03	5.9687E−03	3.0247E−03	0.99586	0.92433	0.98435
19	Gauss2MF	3–2	1.6768E−03	3.3766E−03	2.1283E−03	0.99540	0.97578	0.99225
20	GbellMF	3–2	1.6125E−03	3.6411E−03	2.1753E−03	0.99575	0.97184	0.99191
21	PiMF	3–2	1.5379E−03	3.4438E−03	2.0649E−03	0.99613	0.97481	0.99271
22	PsigMF	3–2	1.5824E−03	2.6110E−03	1.8348E−03	0.99591	0.98552	0.99424
23	TrapMF	3–2	1.6873E−03	4.7358E−03	2.6006E−03	0.99535	0.95236	0.98843
24	TriMF	3–2	1.3585E−03	8.3526E−03	3.9281E−03	0.99698	0.85181	0.97361

properties sit closer to the reference line of zero than that of the linear regression model. This confirms the efficacy of using ANFIS for the modelling of thermophysical properties, as illustrated in previous studies [33, 52, 53].

3.8 Comparison of the thermophysical properties of the present study with prior studies

The ANFIS model developed in this study was compared with existing models from the literature, focusing on varying temperature (15–40 °C) with a nanoparticle loading of 0.1 vol% and varying concentration (0.1–0.4 vol%) at 20 °C. This comparison is illustrated in Figs. 15, 16 and 17 for μ, λ and σ, respectively.

Figure 15a, b illustrates a comparison between the μ concerning concentration and temperature, contrasting the ANFIS model outcome with the predictions generated by models from Kanti et al. [54, 55], Giwa et al. [6] and Dardan et al. [56]. It can be observed that the existing μ models fail to accurately forecast the μ of GNP-Al_2O_3 hybrid nanofluids. Notably, the previously proposed μ models for the GO, GO-Al_2O_3 and MWCNT-Al_2O_3 nanofluids tend to overestimate the data obtained for the current nanofluid. Conversely, when the existing model for Al_2O_3 was applied to predict μ of GNP-Al_2O_3 hybrid nanofluids (Fig. 15a, b), they exhibited a tendency to underestimate the property.

Similarly, the existing proposed models by Kanti et al. [54, 55] struggle to effectively estimate the λ of the current nanofluids, as illustrated in Fig. 16a, b. The model

Table 3 ANFIS architecture optimisation for the nanofluid's electrical conductivity

Run	Model	Number of MFs	RMSE			R-Square		
			Training	Testing	Overall	Training	Testing	Overall
1	DsigMF	2–2	7.68491	24.40743	12.89926	0.99989	0.99857	0.99967
2	GaussMF	2–2	6.00145	18.82015	9.98266	0.99993	0.99915	0.99980
3	Gauss2MF	2–2	7.16815	23.17712	12.18777	0.99990	0.99871	0.99971
4	GbellMF	2–2	6.81794	20.61447	11.05345	0.99991	0.99898	0.99976
5	PiMF	2–2	7.62956	24.41661	12.87642	0.99989	0.99857	0.99967
6	PsigMF	2–2	7.68491	24.40740	12.89924	0.99989	0.99857	0.99967
7	TrapMF	2–2	4.86658	14.32522	7.74527	0.99995	0.99951	0.99988
8	TriMF	2–2	6.11887	17.29217	9.47398	0.99993	0.99928	0.99982
9	DsigMF	2–3	3.55324	16.71019	8.12075	0.99998	0.99933	0.99987
10	GaussMF	2–3	4.02194	17.24760	8.51098	0.99997	0.99929	0.99986
11	Gauss2MF	2–3	4.15525	21.74639	10.41124	0.99997	0.99887	0.99979
12	GbellMF	2–3	3.94662	19.27616	9.31530	0.99997	0.99911	0.99983
13	PiMF	2–3	2.76479	13.25366	6.42240	0.99999	0.99958	0.99992
14	PsigMF	2–3	3.55338	16.71147	8.12132	0.99998	0.99933	0.99987
15	TrapMF	2–3	3.97142	20.72471	9.92575	0.99997	0.99897	0.99980
16	TriMF	2–3	3.90911	14.43096	7.33999	0.99997	0.99950	0.99989
17	DsigMF	3–2	4.18846	11.07197	6.20905	0.99997	0.99971	0.99992
18	GaussMF	3–2	3.21123	12.19721	6.16474	0.99998	0.99964	0.99992
19	Gauss2MF	3–2	3.89521	10.31808	5.78193	0.99997	0.99975	0.99993
20	GbellMF	3–2	3.62355	8.73260	5.07501	0.99998	0.99982	0.99995
21	PiMF	3–2	4.16049	11.02770	6.17817	0.99997	0.99971	0.99992
22	PsigMF	3–2	4.18846	11.07196	6.20904	0.99997	0.99971	0.99992
23	TrapMF	3–2	3.49162	10.71819	5.72093	0.99998	0.99973	0.99994
24	TriMF	3–2	5.59803	17.40269	9.25424	0.99994	0.99928	0.99983

Table 4 Performance of the best three ANFIS architectures for each thermophysical property

Property	ANFIS run	Input MF Type	Number of MFs	Margin of deviation (%)		MSE	MAPE	RMSE	R^2
				Minimum	Maximum				
Viscosity	**14**	**PsigMF**	**2–3**	**− 1.39**	**0.39**	**9.33E−06**	**0.20963**	**0.00306**	**0.99965**
	9	DsigMF	2–3	− 1.39	0.39	9.37E−06	0.21001	0.00306	0.99964
	16	TriMF	2–3	− 1.12	1.02	2.27E−05	0.39473	0.00477	0.99914
Thermal conductivity	**22**	**DsigMF**	**3–2**	**− 0.42**	**0.77**	**3.37E−06**	**0.21925**	**0.00184**	**0.99424**
	17	PsigMF	3–2	− 0.42	0.77	3.37E−06	0.21929	0.00184	0.99424
	21	PiMF	3–2	− 0.42	1.12	4.26E−06	0.22747	0.00207	0.99271
Electrical conductivity	**20**	**GbellMF**	**3–2**	**− 0.75**	**0.79**	**25.75573**	**0.27859**	**5.07501**	**0.99995**
	23	TrapMF	3–2	− 0.78	0.76	32.72904	0.29339	5.72093	0.99994
	19	Gauss2MF	3–2	− 1.11	0.78	33.43066	0.30083	5.78193	0.99993

for GO nanofluid overestimated the current data, while the other existing models (GO-Al$_2$O$_3$ and Al$_2$O$_3$) underestimated the λ of the GNP-Al$_2$O$_3$ hybrid nanofluids.

Additionally, Fig. 17a, b presents the comparison between the σ data from this present study and that which were estimated from existing models, including
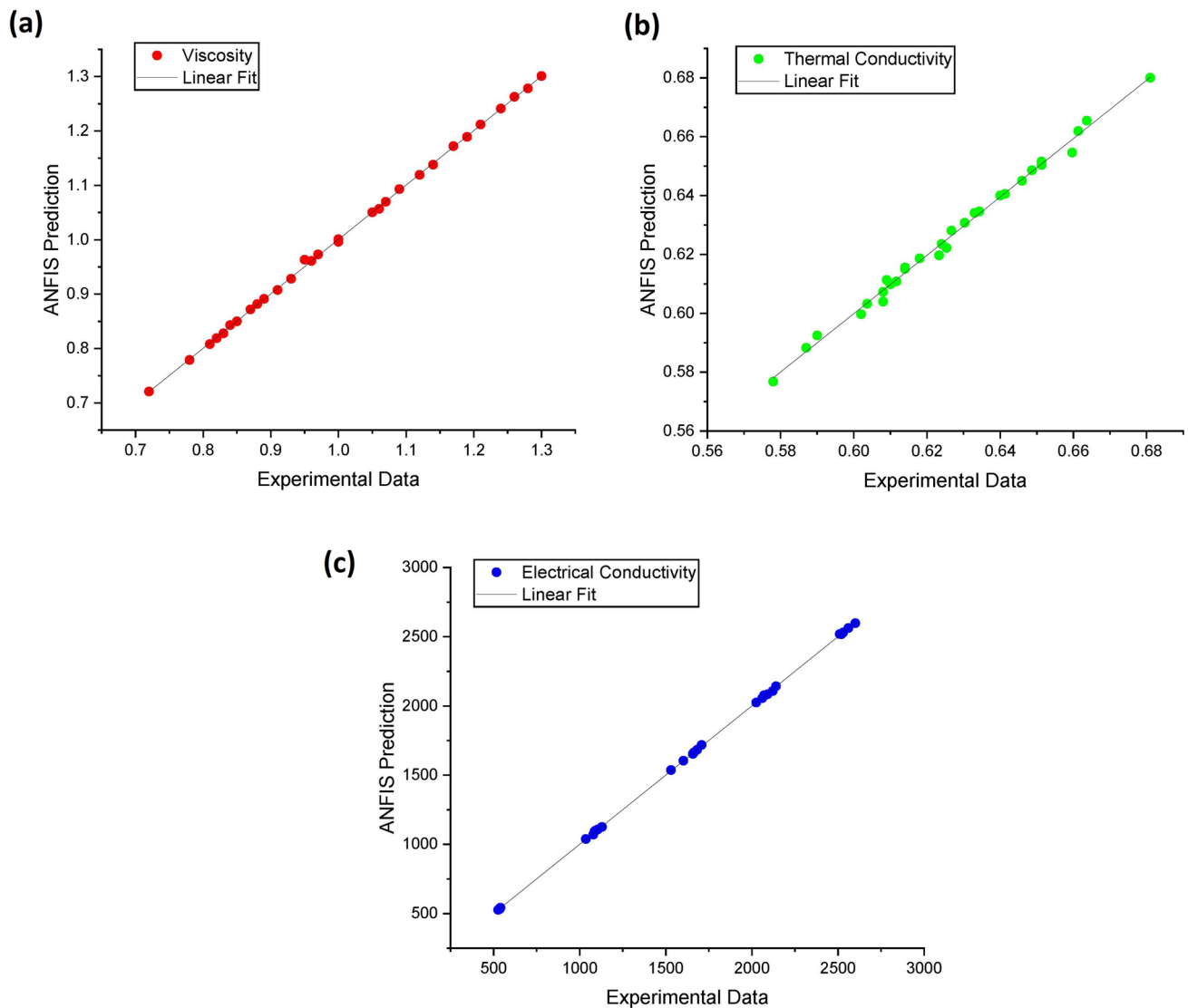
Fig. 12 A linear plot of ANFIS prediction value against the actual values for **a** viscosity, **b** thermal conductivity and **c** electrical conductivity

Minea and Luciu (Al_2O_3 nanofluid) [57], Chereches and Minea (titania nanofluid) [58], and Giwa et al. (MWCNT-Al_2O_3 and Al_2O_3-Fe_2O_3 nanofluids) [6, 59]. Much like the other properties, all the existing models struggled to estimate the σ values of the GNP-Al_2O_3 hybrid nanofluids. The models for Al_2O_3-Fe_2O_3 overestimated the current data, while the other existing model underestimated this study's σ. However, the model from Minea and Luciu (Al_2O_3 nanofluid) [57] was observed to produce

estimates close to the σ of GNP-Al_2O_3 hybrid nanofluids for 0.1 vol% at varying temperatures (Fig. 17b).

The observed disparities between the ANFIS model's predictions and those of existing μ, σ and λ models highlight the unique and complex nature of GNP-Al_2O_3 hybrid nanofluids. These discrepancies can be attributed to several factors. Firstly, the hybrid nature of GNP-Al_2O_3 nanoparticles creates a distinctive interplay of properties, including surface area, shape, and chemical composition, significantly influencing the nanofluid's behaviour.
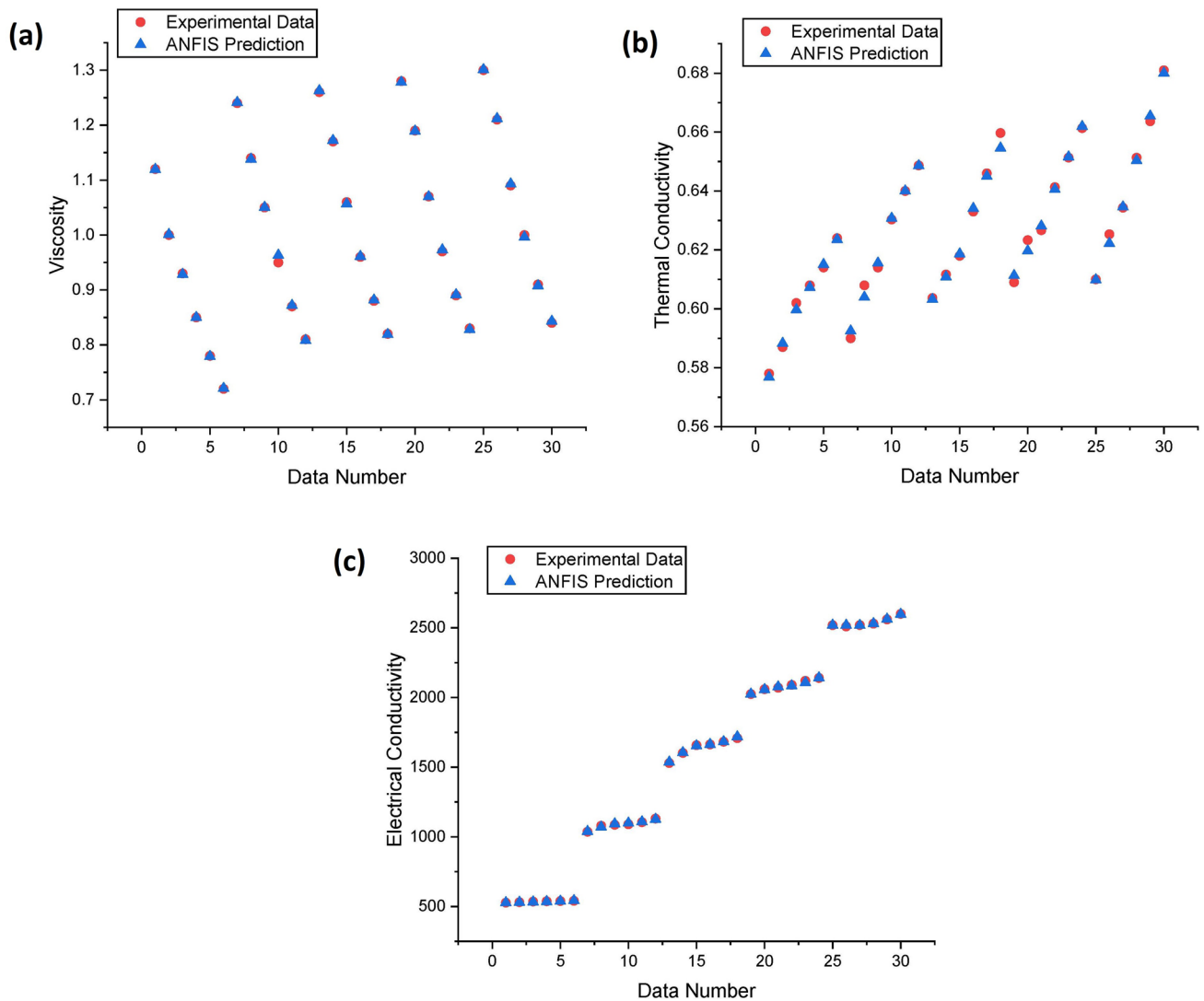
Fig. 13 Comparison of the experimental data and the ANFIS prediction data for **a** viscosity, **b** thermal conductivity and **c** electrical conductivity

Existing models, primarily designed for single-nanoparticle systems or different hybrid combinations, may not adequately capture the intricate interactions within GNP-Al_2O_3 nanofluids. Secondly, the large surface area per unit volume of GNP in the hybrid nanofluid plays a pivotal role in altering the interfacial characteristics and, consequently, the nanofluid's thermophysical properties. This unique feature of GNP-Al_2O_3 nanofluids deviates from the assumptions and parameterisations of existing models, leading to disparities in predictions.

Additionally, the experimental data used for training and validating the ANFIS model are specific to GNP-Al_2O_3 hybrid nanofluids, enabling the model to capture the nuanced relationships within this particular system. In contrast, existing models are often developed based on broader datasets encompassing different nanoparticle types and concentrations, which may not adequately represent the intricacies of GNP-Al_2O_3 nanofluids.

Notwithstanding, it's noteworthy that the nanofluids data from the current study and existing models
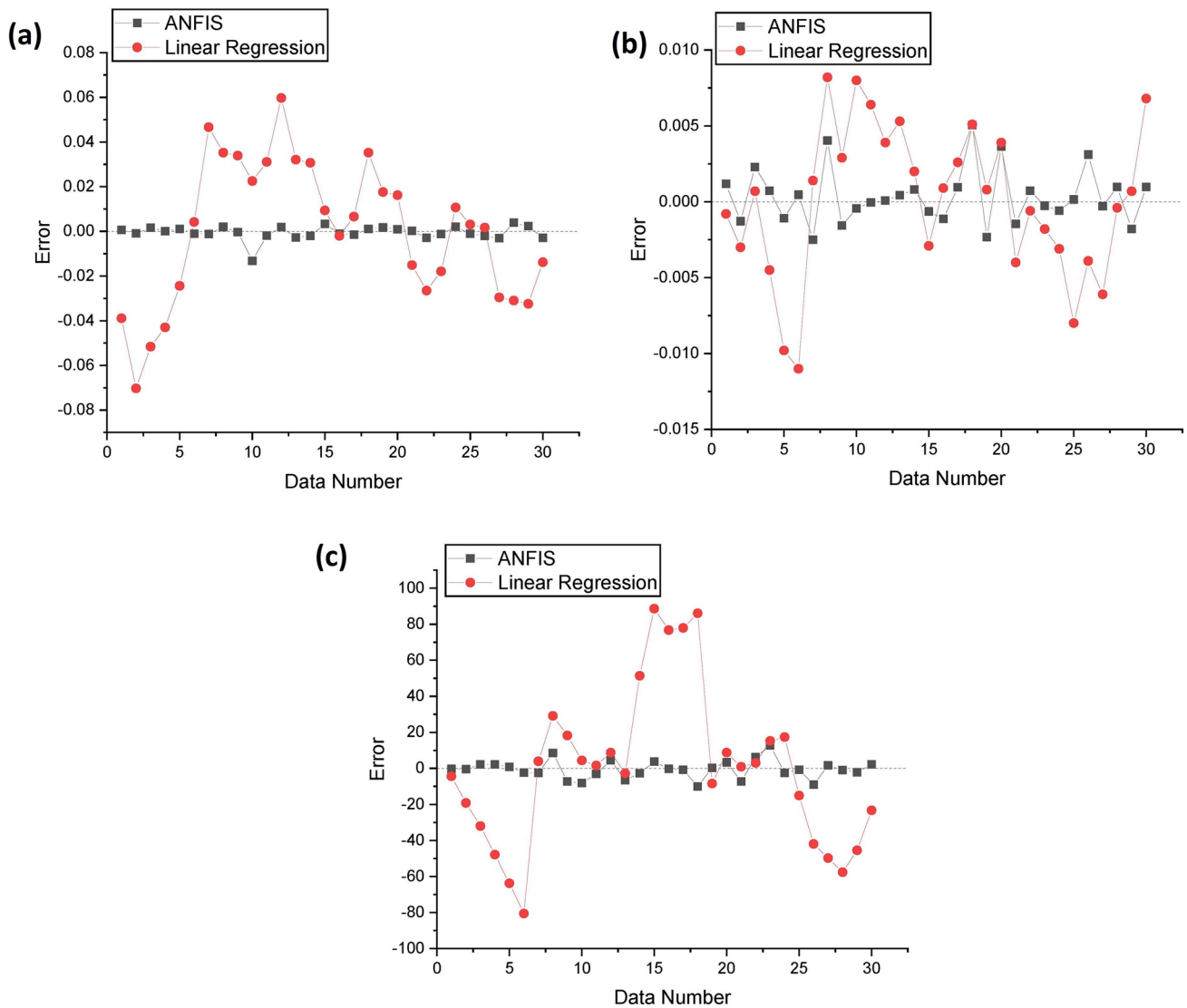
Fig. 14 Comparison of the residuals of the ANFIS prediction model and Linear regression models

consistently demonstrate a similar behaviour. As the concentration of nanoparticles increases, both μ, λ and σ display an upward trend. Conversely, an elevation in temperature corresponds to an increase in λ and σ but a decrease in μ. This pattern underscores the interplay of concentration and temperature in shaping the nanofluid's thermophysical properties.

4 Conclusion

In conclusion, this study investigated the thermophysical properties and heat transfer performance of a hybrid nanofluid composed of GNP and γ-Al_2O_3 nanoparticles dispersed in deionised water across a range of nanoparticle loadings (0.1–0.4 vol%) and temperatures (15–40 °C). The findings underscored the significant increments in λ, μ, and σ as nanoparticle concentration increased. Notably, at the highest nanoparticle concentration (0.4 vol%),
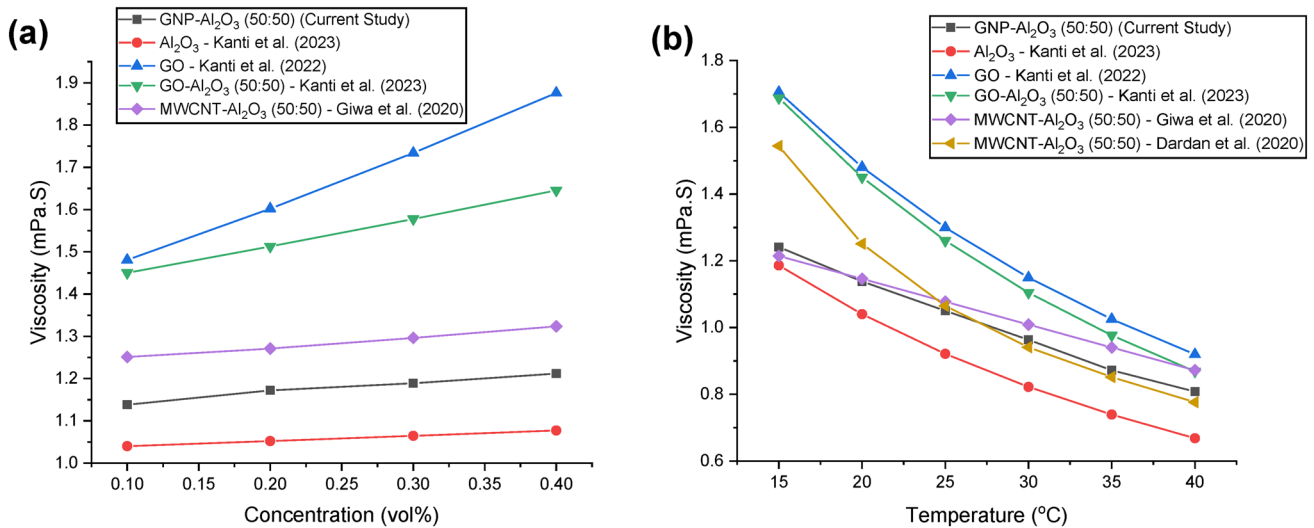
Fig. 15 Comparison of the ANFIS model for viscosity with existing models in literature
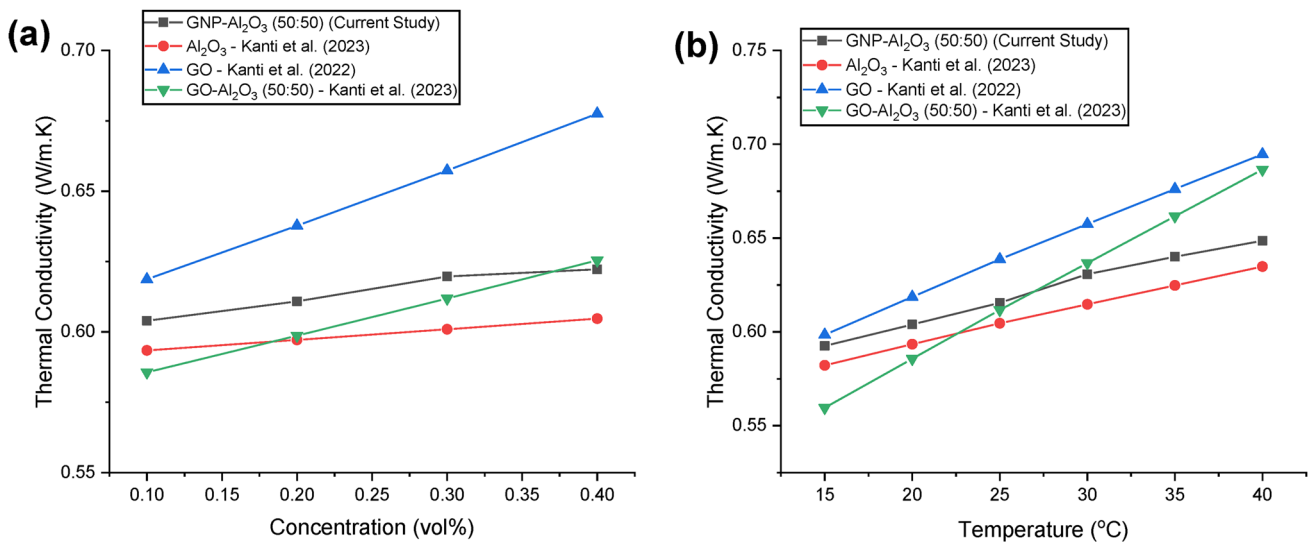
Fig. 16 Comparison of the ANFIS model for thermal conductivity with existing models in literature

the study observed a substantial increment of 21.74% in μ, along with peak enhancements of 17.82% in λ and 393.36% in σ at 40 °C.

The developed correlations and ANFIS models provide robust predictive tools, offering engineers a means to rapidly estimate the hybrid nanofluid's properties. These models exhibited high accuracy, as indicated by R^2 values of 0.9625, 0.9585, and 0.9963 for μ, λ, and σ, respectively.

This exceptional accuracy was achieved with the optimal ANFIS model employing the Product of Sigmas, Difference of Sigmas, and Generalized Bell MFs, with corresponding input numbers of MFs (2–3, 3–2, and 3–2) for μ, λ, and σ, respectively.

Furthermore, the Figure of Merit analysis, incorporating the Mouromtseff Number, identified an optimal nanoparticle concentration range (0.1–0.2 vol%) that balances heat
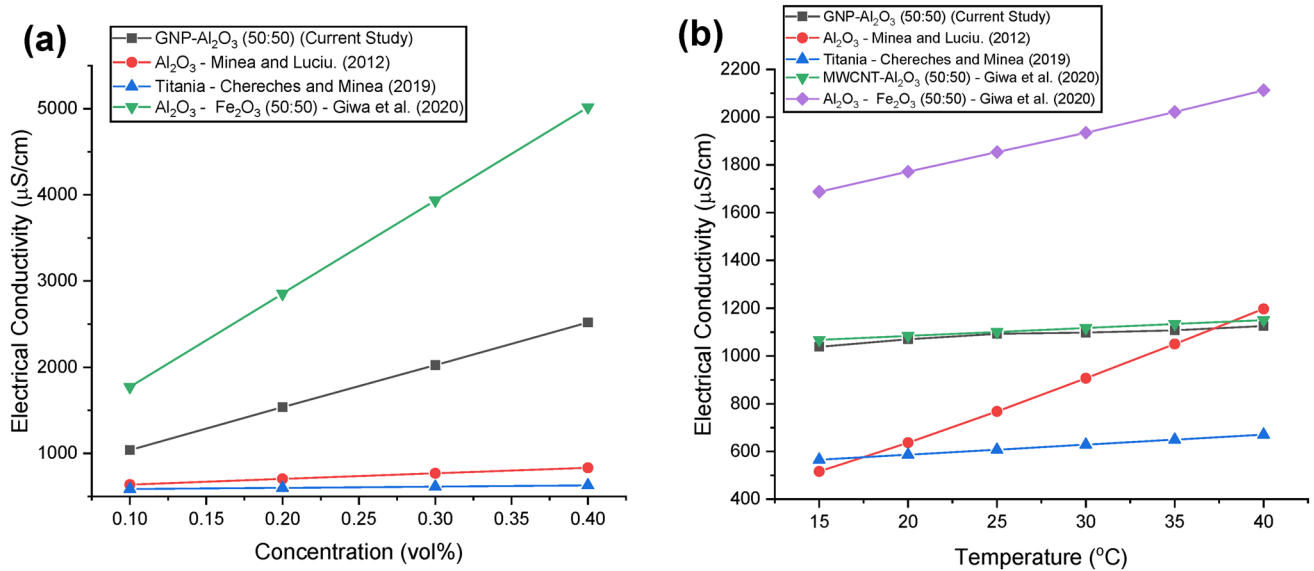
Fig. 17 Comparison of the ANFIS model for electrical conductivity with existing models in literature

transfer enhancements with reasonable μ increments. This valuable guidance can aid practitioners in leveraging the benefits of the hybrid nanofluid while managing potential trade-offs.

Overall, this study's comprehensive analysis of the GNP/Al_2O_3 hybrid nanofluid's thermophysical properties, coupled with the predictive power of correlations and ANFIS modelling, holds promise for advancing thermal management solutions in various industrial applications.

Declarations

References

1. Vakili M, Hosseinalipour SM, Delfani S, Khosrojerdi S, Karami M (2016) Experimental investigation of graphene nanoplatelets nanofluid-based volumetric solar collector for domestic hot water systems. Sol Energy 131:119–130. https://doi.org/10.1016/J.SOLENER.2016.02.034
2. Borode AO, Ahmed NA, Olubambi PA, Sharifpur M, Meyer JP (2021) Effect of various surfactants on the viscosity, thermal and electrical conductivity of graphene nanoplatelets nanofluid. Int J Thermophys 42(11):158. https://doi.org/10.1007/s10765-021-02914-w
3. Devendiran DK, Amirtham VA (2016) A review on preparation, characterisation, properties and applications of nanofluids. Renew Sustain Energy Rev 60:21–40. https://doi.org/10.1016/j.rser.2016.01.055
4. Kazemi I, Sefid M, Afrand M (2020) A novel comparative experimental study on rheological behavior of mono and hybrid nanofluids concerned graphene and silica nano-powders: characterisation, stability and viscosity measurements. Powder Technol 366:216–229. https://doi.org/10.1016/j.powtec.2020.02.010
5. Kazemi I, Sefid M, Afrand M (2020) Improving the thermal conductivity of water by adding mono and hybrid nano-additives containing graphene and silica: a comparative experimental study. Int Commun Heat Mass Transf 116:104648. https://doi.org/10.1016/J.ICHEATMASSTRANSFER.2020.104648

6. Giwa SO, Sharifpur M, Meyer JP (2020) Experimental study of thermo-convection performance of hybrid nanofluids of Al_2O_3-MWCNT/water in a differentially heated square cavity. Int J Heat Mass Transf 148:119072. https://doi.org/10.1016/j.ijheatmasstransfer.2019.119072

7. Nagarajan FC, Kannaiyan SK, Boobalan C (2020) Intensification of heat transfer rate using alumina-silica nanocoolant. Int J Heat Mass Transf 149:119127. https://doi.org/10.1016/j.ijheatmasstransfer.2019.119127

8. Allahyar HR, Hormozi F, ZareNezhad B (2016) Experimental investigation on the thermal performance of a coiled heat exchanger using a new hybrid nanofluid. Exp Therm Fluid Sci 76:324–329. https://doi.org/10.1016/j.expthermflusci.2016.03.027

9. Giwa SO, Sharifpur M, Ahmadi MH, Sohel Murshed SM, Meyer JP (2021) Experimental investigation on stability, viscosity, and electrical conductivity of water-based hybrid nanofluid of MWCNT-Fe_2O_3. Nanomaterials 11(1):136

10. Gulzar O, Qayoum A, Gupta R (2021) Experimental study on thermal conductivity of mono and hybrid Al_2O_3–TiO_2 nanofluids for concentrating solar collectors. Int J Energy Res 45(3):4370–4384. https://doi.org/10.1002/ER.6105

11. Borode A, Tshephe T, Olubambi P, Sharifpur M, Meyer J (2023) Stability and thermophysical properties of GNP-Fe_2O_3 hybrid nanofluid: effect of volume fraction and temperature. Nanomaterials. https://doi.org/10.3390/nano13071238

12. Said Z, Jamei M, Syam Sundar L, Pandey AK, Allouhi A, Li C (2022) Thermophysical properties of water, water and ethylene glycol mixture-based nanodiamond + Fe_3O_4 hybrid nanofluids: An experimental assessment and application of data-driven approaches. J Mol Liq 347:117944. https://doi.org/10.1016/j.molliq.2021.117944

13. Shajan S, Baiju V, Krishnakumar TS et al (2021) Experimental investigation on thermophysical properties of Therminol® 55 based hybrid nanofluids with alumina and graphene nanoplatelets for medium temperature applications. Therm Sci Eng Prog 26:101116. https://doi.org/10.1016/j.tsep.2021.101116

14. Said Z, Sharma P, Syam Sundar L, Afzal A, Li C (2021) Synthesis, stability, thermophysical properties and AI approach for predictive modelling of Fe_3O_4 coated MWCNT hybrid nanofluids. J Mol Liq 340:117291. https://doi.org/10.1016/j.molliq.2021.117291

15. Li X, Wang H, Luo B (2021) The thermophysical properties and enhanced heat transfer performance of SiC-MWCNTs hybrid nanofluids for car radiator system. Colloids Surf A Physicochem Eng Asp 612:125968. https://doi.org/10.1016/j.colsurfa.2020.125968

16. Urmi W, Rahman MM, Hamzah WAW (2020) An experimental investigation on the thermophysical properties of 40% ethylene glycol based TiO_2–Al_2O_3 hybrid nanofluids. Int Commun Heat Mass Transf 116:104663. https://doi.org/10.1016/j.icheatmasstransfer.2020.104663

17. Wanatasanappan VV, Abdullah MZ, Gunnasegaran P (2020) Thermophysical properties of Al_2O_3-CuO hybrid nanofluid at different nanoparticle mixture ratio: an experimental approach. J Mol Liq 313:113458. https://doi.org/10.1016/j.molliq.2020.113458

18. Aybar H, Sharifpur M, Azizian MR, Mehrabi M, Meyer JP (2015) A review of thermal conductivity models for nanofluids. Heat Transf Eng 36(13):1085–1110. https://doi.org/10.1080/01457632.2015.987586

19. Hemmat Esfe M, Kamyab MH, Toghraie D (2022) Statistical review of studies on the estimation of thermophysical properties of nanofluids using artificial neural network (ANN). Powder Technol 400:117210. https://doi.org/10.1016/j.powtec.2022.117210

20. Sedaghat F, Yousefi F (2019) Synthesises, characterisation, measurements and modeling thermal conductivity and viscosity of graphene quantum dots nanofluids. J Mol Liq 278:299–308. https://doi.org/10.1016/J.MOLLIQ.2019.01.073

21. Tian S, Arshad NI, Toghraie D, Eftekhari SA, Hekmatifar M (2021) Using perceptron feed-forward Artificial Neural Network (ANN) for predicting the thermal conductivity of graphene oxide-Al_2O_3/water-ethylene glycol hybrid nanofluid. Case Stud Therm Eng 26:101055. https://doi.org/10.1016/J.CSITE.2021.101055

22. Yashawantha KM, Vinod AV (2021) ANFIS modelling of effective thermal conductivity of ethylene glycol and water nanofluids for low temperature heat transfer application. Therm Sci Eng Prog 24:100936. https://doi.org/10.1016/j.tsep.2021.100936

23. Zhang Z, Al-Bahrani M, Ruhani B et al (2023) Optimised ANFIS models based on grid partitioning, subtractive clustering, and fuzzy C-means to precise prediction of thermophysical properties of hybrid nanofluids. Chem Eng J 471:144362. https://doi.org/10.1016/j.cej.2023.144362

24. Vakili M, Khosrojerdi S, Aghajannezhad P, Yahyaei M (2017) A hybrid artificial neural network-genetic algorithm modeling approach for viscosity estimation of graphene nanoplatelets nanofluid using experimental data. Int Commun Heat Mass Transf 82:40–48. https://doi.org/10.1016/j.icheatmasstransfer.2017.02.003

25. Sahin F, Genc O, Gökcek M, Çolak AB (2023) An experimental and new study on thermal conductivity and zeta potential of Fe_3O_4/water nanofluid: Machine learning modeling and proposing a new correlation. Powder Technol 420:118388. https://doi.org/10.1016/j.powtec.2023.118388

26. Alrashed AAAA, Gharibdousti MS, Goodarzi M, de Oliveira LR, Safaei MR, Bandarra Filho EP (2018) Effects on thermophysical properties of carbon based nanofluids: Experimental data, modelling using regression, ANFIS and ANN. Int J Heat Mass Transf 125:920–932. https://doi.org/10.1016/j.ijheatmasstransfer.2018.04.142

27. Amani P, Vajravelu K (2018) Intelligent modeling of rheological and thermophysical properties of green covalently functionalised graphene nanofluids containing nanoplatelets. Int J Heat Mass Transf 120:95–105. https://doi.org/10.1016/j.ijheatmasstransfer.2017.12.025

28. Yadav D, Naruka DS, Singh PK (2021) The insight flow characteristics of concentrated MWCNT in water base fluid: experimental study and ANN modelling. Heat Mass Transf 57(11):1829–1844. https://doi.org/10.1007/s00231-021-03086-x

29. Yan SR, Kalbasi R, Nguyen Q, Karimipour A (2020) Rheological behavior of hybrid MWCNTs-TiO2/EG nanofluid: a comprehensive modeling and experimental study. J Mol Liq 308:113058. https://doi.org/10.1016/J.MOLLIQ.2020.113058

30. AbuShanab Y, Al-Ammari WA, Gowid S, Sleiti AK (2023) Accurate prediction of dynamic viscosity of polyalpha-olefin boron nitride nanofluids using machine learning. Heliyon 9(6):e16716. https://doi.org/10.1016/j.heliyon.2023.e16716

31. ASHRAE (2009) ASHRAE Handbook—Fundamentals (SI Edition). American Society of Heating, Refrigerating and Air-Conditioning Engineers, Inc

32. Jang JSR (1993) ANFIS: adaptive-network-based fuzzy inference system. IEEE Trans Syst Man Cybern 23(3):665–685. https://doi.org/10.1109/21.256541

33. Hemmat Esfe M (2018) Thermal conductivity modeling of aqueous CuO nanofluids by adaptive neuro-fuzzy inference system (ANFIS) using experimental data. Period Polytech Chem Eng 62(2):202–208. https://doi.org/10.3311/PPCH.9670

34. Aylı E (2020) Modeling of mixed convection in an enclosure using multiple regression, artificial neural network, and adaptive neuro-fuzzy interface system models. Proc Inst Mech Eng Part C J Mech

Eng Sci 234(15):3078–3093. https://doi.org/10.1177/0954406220914330

35. Kisi O, Alizamir M, Docheshmeh Gorgij A (2020) Dissolved oxygen prediction using a new ensemble method. Environ Sci Pollut Res 27(9):9589–9603. https://doi.org/10.1007/s11356-019-07574-w

36. Abonyi J, Andersen H, Nagy L, Szeifert F (1999) Inverse fuzzy-process-model based direct adaptive control. Math Comput Simul 51(1):119–132. https://doi.org/10.1016/S0378-4754(99)00142-1

37. Babanezhad M, Nakhjiri AT, Shirazian S (2020) Changes in the number of membership functions for predicting the gas volume fraction in two-phase flow using grid partition clustering of the ANFIS Method. ACS Omega 5(26):16284–16291. https://doi.org/10.1021/acsomega.0c02117

38. Salleh MNM, Talpur N, Talpur KH (2018) A modified neuro-fuzzy system using metaheuristic approaches for data classification. In: Aceves-Fernandez MA, (ed) IntechOpen; 2018:Ch. 2. https://doi.org/10.5772/intechopen.75575

39. Borode AO, Ahmed NA, Olubambi PA (2019) A review of heat transfer application of carbon-based nanofluid in heat exchangers. Nano-Struct Nano Obj 20:100394. https://doi.org/10.1016/j.nanoso.2019.100394

40. Eibl P, Rustige S, Witz C, Khinast J (2020) Chapter four—LBM for two-phase (bio-)reactors. In: Van den Akker HEABTA in CE (ed) Lattice Boltzmann modeling for chemical engineering, vol 55. Academic Press, pp 219–285. https://doi.org/10.1016/bs.ache.2020.04.003

41. Bhuiyan MHU, Saidur R, Amalina MA, Mostafizur RM, Islam A (2015) Effect of nanoparticles concentration and their sizes on surface tension of nanofluids. Procedia Eng 105:431–437. https://doi.org/10.1016/j.proeng.2015.05.030

42. Bahrami M, Akbari M, Karimipour A, Afrand M (2016) An experimental study on rheological behavior of hybrid nanofluids made of iron and copper oxide in a binary mixture of water and ethylene glycol: non-Newtonian behavior. Exp Therm Fluid Sci 79:231–237. https://doi.org/10.1016/J.EXPTHERMFLUSCI.2016.07.015

43. Murshed SMS, Leong KC, Yang C (2008) Thermophysical and electrokinetic properties of nanofluids—a critical review. Appl Therm Eng 28(17):2109–2125. https://doi.org/10.1016/j.applthermaleng.2008.01.005

44. Kumar PM, Kumar J, Tamilarasan R, Sendhilnathan S, Suresh S (2015) Review on nanofluids theoretical thermal conductivity models. Eng J (Eng J) 19(1 SE-Modern Engineering Technology):234. https://doi.org/10.4186/ej.2015.19.1.67

45. Taherian H, Alvarado JL, Languri EM (2018) Enhanced thermophysical properties of multiwalled carbon nanotubes based nanofluids. Part 2: experimental verification. Renew Sustain Energy Rev 82:4337–4344. https://doi.org/10.1016/j.rser.2017.05.117

46. Khairul MA, Shah K, Doroodchi E, Azizian R, Moghtaderi B (2016) Effects of surfactant on stability and thermo-physical properties of metal oxide nanofluids. Int J Heat Mass Transf 98:778–787. https://doi.org/10.1016/J.IJHEATMASSTRANSFER.2016.03.079

47. Giwa SO, Sharifpur M, Meyer JP, Wongwises S, Mahian O (2021) Experimental measurement of viscosity and electrical conductivity of water-based γ-Al2O3/MWCNT hybrid nanofluids with various particle mass ratios. J Therm Anal Calorim 143(2):1037–1050. https://doi.org/10.1007/s10973-020-10041-1

48. Ijam A, Saidur R, Ganesan P, Moradi Golsheikh A (2015) Stability, thermo-physical properties, and electrical conductivity of graphene oxide-deionised water/ethylene glycol based nanofluid. Int J Heat Mass Transf 87:92–103. https://doi.org/10.1016/J.IJHEATMASSTRANSFER.2015.02.060

49. Minea AA, Moldoveanu MG (2017) Studies on Al$_2$O$_3$, CuO, and TiO$_2$ water-based nanofluids: a comparative approach in laminar and turbulent flow. J Eng Thermophys 26(2):291–301. https://doi.org/10.1134/S1810232817020114

50. Borode AO, Ahmed NA, Olubambi PA, Sharifpur M, Meyer JP (2021) Investigation of the thermal conductivity, viscosity, and thermal performance of graphene nanoplatelet-alumina hybrid nanofluid in a differentially heated cavity. Front Energy Res 9:482. https://doi.org/10.3389/fenrg.2021.737915

51. Huminic G, Huminic A (2018) Heat transfer capability of the hybrid nanofluids for heat transfer applications. J Mol Liq 272:857–870. https://doi.org/10.1016/j.molliq.2018.10.095

52. Mehrabi M, Sharifpur M, Meyer JP (2013) Viscosity of nanofluids based on an artificial intelligence model. Int Commun Heat Mass Transf 43:16–21. https://doi.org/10.1016/J.ICHEATMASSTRANSFER.2013.02.008

53. Alarifi IM, Nguyen HM, Bakhtiyari AN, Asadi A (2019) Feasibility of ANFIS-PSO and ANFIS-GA models in predicting thermophysical properties of Al$_2$O$_3$-MWCNT/oil hybrid nanofluid. Mater 12(21):3628. https://doi.org/10.3390/MA12213628

54. Kanti P, Sharma KV, Khedkar RS, Rehman T, ur (2022) Synthesis, characterisation, stability, and thermal properties of graphene oxide based hybrid nanofluids for thermal applications: experimental approach. Diam Relat Mater 128:109265. https://doi.org/10.1016/J.DIAMOND.2022.109265

55. Kanti PK, Sharma P, Maiya MP, Sharma KV (2023) The stability and thermophysical properties of Al$_2$O$_3$-graphene oxide hybrid nanofluids for solar energy applications: application of robust autoregressive modern machine learning technique. Sol Energy Mater Sol Cells 253:112207. https://doi.org/10.1016/J.SOLMAT.2023.112207

56. Dardan E, Afrand M, Meghdadi Isfahani AH (2016) Effect of suspending hybrid nano-additives on rheological behavior of engine oil and pumping power. Appl Therm Eng 109:524–534. https://doi.org/10.1016/j.applthermaleng.2016.08.103

57. Minea AA, Luciu RS (2012) Investigations on electrical conductivity of stabilised water based Al$_2$O$_3$ nanofluids. Microfluid Nanofluid 13(6):977–985. https://doi.org/10.1007/S10404-012-1017-4

58. Chereches EI, Minea AA (2019) Electrical conductivity of new nanoparticle enhanced fluids: an experimental study. Nanomater (Basel, Switzerland). https://doi.org/10.3390/nano9091228

59. Giwa SO, Sharifpur M, Goodarzi M, Alsulami H, Meyer JP (2021) Influence of base fluid, temperature, and concentration on the thermophysical properties of hybrid nanofluids of alumina–ferrofluid: experimental data, modeling through enhanced ANN, ANFIS, and curve fitting. J Therm Anal Calorim 143(6):4149–4167. https://doi.org/10.1007/s10973-020-09372-w